Cell Reports

Article

Active Tonic mTORC1 Signals Shape Baseline Translation in Naive T Cells

Graphical Abstract

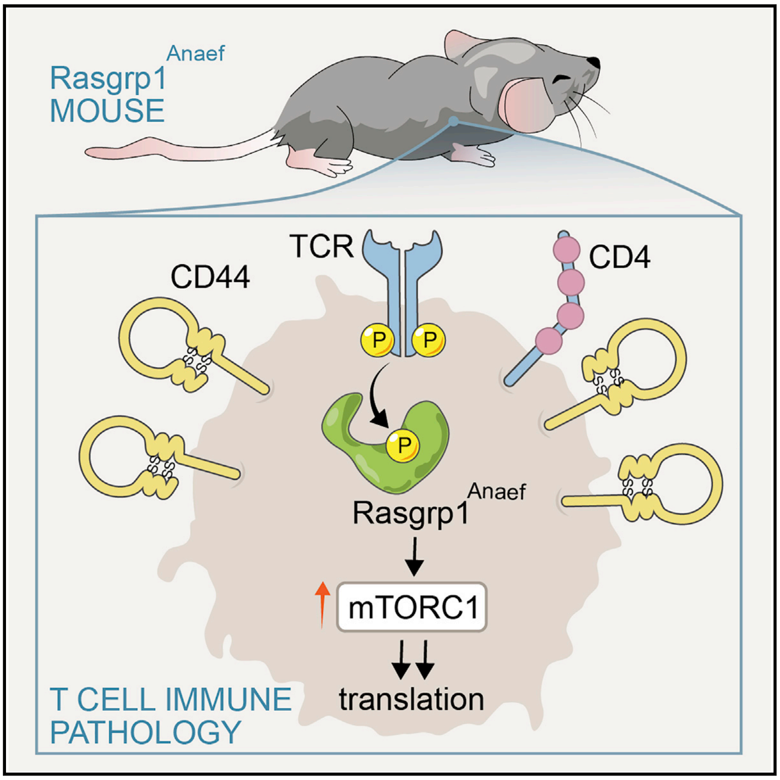

Authors

Darienne R. Myers, Emilia Norlin,
Yvonne Vercoulen, Jeroen P. Roose

Correspondence

jeroen.roose@ucsf.edu

In Brief

Myers et al. evaluate a mouse model of autoimmunity, Rasgrp1^{Anaef}. They find that T cells with the Rasgrp1^{Anaef} allele exhibit altered signaling from Rasgrp1 to the mTORC1 pathway in the basal state. They show that increased basal Rasgrp1^{Anaef}-mTORC1 signals lead to an altered translational landscape in T cells and immunopathology.

Highlights

- Naive, resting CD4$^+$ T cells display selective, robust tonic mTORC1 signals
- The Ras exchange factor Rasgrp1 is necessary to drive tonic mTORC1 signals
- Tonic mTORC1 signals affect the baseline translational landscape of primary T cells
- *Rasgrp1^{Anaef}* causes immunopathology and translation changes in T cells

Myers et al., 2019, Cell Reports *27*, 1858–1874
May 7, 2019 © 2019 The Author(s).
https://doi.org/10.1016/j.celrep.2019.04.037

OPEN
ACCESS
CellPress

Cell Reports
Article

Active Tonic mTORC1 Signals Shape Baseline Translation in Naive T Cells

Darienne R. Myers,[1,2] Emilia Norlin,[1] Yvonne Vercoulen,[1,3] and Jeroen P. Roose[1,4,*]
[1]Department of Anatomy, University of California, San Francisco, San Francisco, CA 94143, USA
[2]Present address: Revolution Medicines, Redwood City, CA 94063, USA
[3]Present address: Molecular Cancer Research, Center for Molecular Medicine, UMC Utrecht, Utrecht University, Utrecht, the Netherlands
[4]Lead Contact
*Correspondence: jeroen.roose@ucsf.edu

https://doi.org/10.1016/j.celrep.2019.04.037

SUMMARY

Naive CD4$^+$ T cells are an example of dynamic cell homeostasis: T cells need to avoid autoreactivity while constantly seeing self-peptides, yet they must be primed to react to foreign antigens during infection. The instructive signals that balance this primed yet quiescent state are unknown. Interactions with self-peptides result in membrane-proximal, tonic signals in resting T cells. Here we reveal selective and robust tonic mTORC1 signals in CD4$^+$ T cells that influence T cell fate decisions. We find that the Ras exchange factor Rasgrp1 is necessary to generate tonic mTORC1 signals. Genome-wide ribosome profiling of resting, primary CD4$^+$ T cells uncovers a baseline translational landscape rich in mTOR targets linked to mitochondria, oxidative phosphorylation, and splicing. Aberrantly increased tonic mTORC1 signals from a *Rasgrp1^{Anaef}* allele result in immunopathology with spontaneous appearance of T peripheral helper cells, follicular helper T cells, and anti-nuclear antibodies that are preceded by subtle alterations in the translational landscape.

INTRODUCTION

Under healthy homeostatic conditions, patrolling T cells encounter self-peptides (self-p). Importantly, these contacts with self-p-MHC must not trigger full T cell activation to avoid autoimmunity (Hogquist et al., 2003, 2005). Both CD4$^+$ and CD8$^+$ primary T cells exhibit sub-threshold signaling, which we here term ‘‘tonic signaling’’ (Myers et al., 2017b). Continuous interactions of the T cell receptor (TCR) with self-p-MHC are critical for the generation of these tonic signals, as administration of a blocking antibody to MHC class II or transfer of cells into class II-deficient hosts led to reduced T cell responses upon stimulation (Stefanová et al., 2002). Work from the early 1990s revealed that proximal signaling molecules such as the TCR zeta chain (TCRζ) immunoreceptor tyrosine-based activation motifs (ITAMs) (van Oers et al., 1993) are phosphorylated in the basal state, and the Syk family kinase Zap70 associates with pTCRζ (van Oers et al., 1994). The cell surface molecule CD5 has been used as a marker of tonic proximal TCR signaling (Azzam et al., 1998). In follow-up studies more than a decade later, it was demonstrated that CD4$^+$ T cells as well as CD8$^+$ T cells with the highest CD5 expression (and thus highest tonic signals) are the best T cell responders during bacterial and viral infections (Fulton et al., 2015; Mandl et al., 2013). On the basis of these studies, a hypothesis formed that tonic signals may establish a primed yet controlled state in primary T cells (Mandl et al., 2013; Myers et al., 2017a, 2017b; Persaud et al., 2014), but molecular insights into tonic signaling pathways and functional outputs have been lacking. Rasgrp1 (Ras guanyl nucleotide releasing protein 1) is a Ras guanine nucleotide exchange factor (RasGEF) (Ksionda et al., 2013). In resting cells, Rasgrp1 predominantly takes on an autoinhibited homodimer conformation (Iwig et al., 2013). We previously reported a mouse model carrying a point-mutated Rasgrp1 allele (*Rasgrp1^{Anaef}*; R519G substitution, hereafter termed ‘‘Anaef’’). Our studies on the Anaef mouse model with immunopathology suggested that basal mTOR activity may affect the resting state *in vivo* (Daley et al., 2013).

mTOR (mechanistic-mammalian target of rapamycin) is a serine-threonine kinase that is a well-defined sensor of environmental cues: its activity is known to be induced by input from receptors, soluble factors such as cytokines, and amino acids (Laplante and Sabatini, 2012; Powell and Delgoffe, 2010; Saxton and Sabatini, 2017). There is increased interest in the role of mTOR signaling in CD4$^+$ T cell biology (Chi, 2012; Delgoffe et al., 2009, 2011; Heikamp et al., 2014; Piccirillo et al., 2014; Powell et al., 2012; So et al., 2016; Waickman and Powell, 2012; Yang et al., 2013, 2016; Zeng et al., 2016; Zhang et al., 2011). Whether mTOR has important functions in the basal state, under conditions of tonic signaling, is not known.

mTOR associates with cofactors and accessory proteins to form two distinct, active kinase complexes, mTORC1 and mTORC2 (Zoncu et al., 2011). Known mTORC1 substrates are S6K1/2 and 4E-BP1/2/3, while mTORC2 phosphorylates Akt and other SGK family members. mTOR signaling downstream of these substrates regulates processes such as cell growth, metabolism, and translation of mRNAs into proteins (Chi, 2012; Laplante and Sabatini, 2012). The role of mTOR signaling in translation has been investigated using *in vitro* proliferating cells or transformed cancer cell lines. In 2012, two studies established mTOR translation signatures using ribosome profiling. Capitalizing on a Torin 1 kinase inhibitor, mTORC1-mediated regulation of mRNA translation was revealed in proliferating, P53-deficient

© 2019 The Author(s).
This is an open access article under the CC BY-NC-ND license (http://creativecommons.org/licenses/by-nc-nd/4.0/).

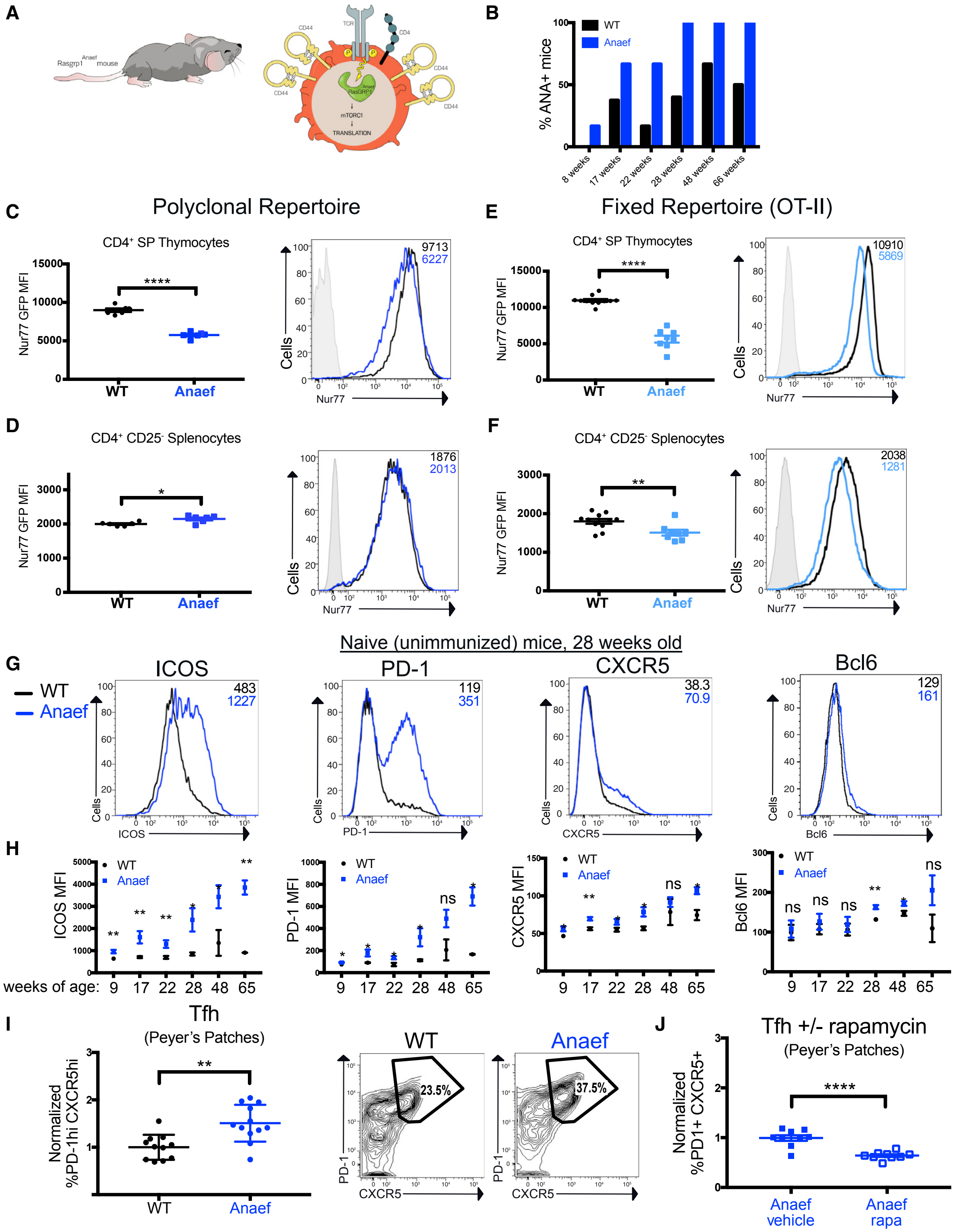

Figure 1. Aberrant Rasgrp1^{Anaef} Signals and T Cell-Mediated Autoimmunity

(A) Cartoon summarizing the phenotype of the Rasgrp1^{Anaef} mouse, which has elevated CD44 on CD4^{+} T cells and increased basal mTORC1 signaling.

(B) HEp-2 anti-nuclear antibody (ANA) assay on serum from WT and Anaef mice at the indicated ages. Data are percentage of mice at each age that scored positive for ANAs. Data are from one experiment with two to six mice per genotype per age.

(legend continued on next page)

mouse embryonic fibroblasts (MEFs) (Thoreen et al., 2012), and ribosome profiling of a proliferating human prostate cancer cell line PC3 revealed 144 target mRNAs that changed upon INK128 kinase inhibitor treatment (Hsieh et al., 2012).

Here, we demonstrate that primary naive CD4$^+$ T cells display robust and selective tonic activity through the mTORC1-S6 signaling pathway that shapes the baseline translational landscape in resting T cells *in vivo*. Subtle alterations in this landscape in *Rasgrp1*^{Anaef} T cells precede spontaneous cell fate trajectories toward T peripheral helper cells and follicular helper T cells, as well as other immunopathological features.

RESULTS

Aberrant Rasgrp1^{Anaef}-mTORC1 Signals and T Cell-Mediated Autoimmunity

Tonic signaling relies on frequent, transient contacts of TCRs with self-p-MHC in lymphoid organs (Fulton et al., 2015; Hogquist et al., 2003; Mandl et al., 2013; Markegard et al., 2011; Myers et al., 2017b; Oki-Idouchi and Lorenzo, 2007; Stefanová et al., 2002; van Oers et al., 1993, 1994). A major challenge in tonic signaling studies has been that the molecules and therefore mechanisms that control the "fitness" or "primed state" have remained elusive (Myers et al., 2017b). We recently described how tonic signals put the brake on naive T cells to prevent aberrant basal activity through a tonic linker for activation of T cells (LAT)-HDAC7 signal that maintains mRNA expression of a cluster of genes that are negative regulators of T cell proliferation and differentiation (Myers et al., 2017a). A *Rasgrp1*^{Anaef} mouse pointed us to a possible counterbalancing function of tonic signaling: promoting T cell activity in the basal state. We also identified a possible role for mTORC1 signaling in this "promoting" function (Daley et al., 2013).

Two studies suggested that the RasGEF Rasgrp1 might be involved in mTORC1 signaling (Daley et al., 2013; Gorentla et al., 2011). Naive CD4$^+$ Rasgrp1^{Anaef} T cells exhibit elevated basal mTORC1 signaling and a selective increase in CD44 expression (Figure 1A; Daley et al., 2013), likely through reduced autoinhibition in the Rasgrp1^{Anaef} molecule. These mice exhibit immunopathology such as serum anti-nuclear antibodies (ANAs) and aberrantly high expression of the activation marker CD44. These features are also penetrant when B cells in the *Rasgrp1*^{Anaef} model carry a wild-type *Rasgrp1* allele, implying a *Rasgrp1*^{Anaef} T cell-intrinsic effect (Daley et al., 2013).

Examining serum from wild type (WT) and Anaef mice in a new, longitudinal analysis, we first determined that the spontaneous appearance of ANAs already becomes fully penetrant in Anaef mice on a C57BL/6 background at 28 weeks of age, though ANAs can be observed as early as 8 weeks (Figure 1B). H&E-stained sections of kidneys, a target organ in lupus nephritis, revealed prominent lymphoid aggregates in three of five 66-week-old Anaef mice (data not shown). We observed an increase in isotype-switched serum antibodies in Anaef mice (immunoglobulin G 1 [IgG1], IgG2, IgG3, and IgE), increases in IgM levels, but no differences in IgA (Figure S1A). Thus, B cells in Anaef mice have undergone class switching from IgM to other isotypes, a process that requires T cell help, to a greater extent than in WT mice.

Thymocyte development is mostly intact in Anaef mice, and as such these animals are never lymphopenic. Thymocyte subsets and residence time in the thymus are undistinguishable from WT (Daley et al., 2013). There is a very modest decrease in positive selection and no change in negative selection (Daley et al., 2013). The Anaef allele leads to reduced *in vitro* TCR-induced Erk signaling, and Ras-Erk signaling is known to drive positive selection (Fischer et al., 2005). We wanted to explore if developing Anaef thymocytes select for a more highly self-reactive TCR repertoire, as a means of compensating for the weaker TCR-induced Erk signaling. We crossed Anaef mice to Nur77-GFP reporter mice and analyzed these on both a polyclonal TCR repertoire and on a fixed repertoire (the OTII transgenic TCR). Nur77 expression relies on Erk signaling (van den Brink et al., 1999), and antigen receptors with higher affinity for self drive higher Nur77-GFP expression (Moran et al., 2011; Zikherman et al., 2012). Single-positive (SP) CD4$^+$ thymocytes from Anaef mice on a polyclonal TCR repertoire displayed reduced levels of Nur77-GFP compared with WT counterparts (Figure 1C), in agreement with the previously reported Erk signaling defect in Anaef cells (Daley et al., 2013). Analyzing mature CD4$^+$ T cells in

---

(C) Flow cytometric analysis of CD4 single-positive (SP) thymocytes from WT and Anaef Nur77-GFP mice with a polyclonal T cell receptor (TCR) repertoire. Total thymocytes were first gated to exclude non-T-lineage cells, then on CD4$^+$ CD8$^-$ cells. Data are representative of three independent experiments with three to five mice per group, and error bars represent SEM.

(D) Flow cytometric analysis of splenic CD4$^+$ CD25$^-$ T cells from WT and Anaef Nur77-GFP mice with a polyclonal TCR repertoire. Data are representative of five independent experiments with three to five mice per group. Error bars represent SEM.

(E) As in (C) but with WT and Anaef mice carrying the OT-II TCR transgene to fix the TCR repertoire. Data are representative of three independent experiments with three to five mice per group. Error bars represent SEM.

(F) As in (D) but with all mice carrying the OT-II TCR transgene. Data are representative of three independent experiments with three to five mice per group. Error bars represent SEM.

(G) Flow cytometric analysis of ICOS, PD-1, CXCR5, and Bcl6 protein levels (mean fluorescence intensity [MFI]) on splenic WT and Anaef CD4$^+$ T cells from 28-week-old mice. Data are representative of one experiment with four mice per genotype.

(H) As in (G) but with MFI calculated for mice at the indicated ages. Statistical significance for each age was determined using an unpaired t test, and error bars represent SEM. Data are from one experiment with two to six mice per genotype per age.

(I) Flow cytometric analysis of Tfh cells (gated on CD4$^+$ CD25$^-$ PD1^{hi} CXCR5^{hi}) isolated from Peyer's patches of 28-week-old WT and Anaef mice. Data are representative of four independent experiments with two or three mice per genotype per experiment. Statistics were calculated using unpaired t test; mean ± SEM.

(J) Flow cytometric analysis of Tfh cells (gated on CD4$^+$ CD25$^-$ PD1^{hi} CXCR5^{hi}) isolated from Peyer's patches of 12-week-old Anaef mice treated for 1 week with vehicle or rapamycin (0.4 mg/kg, intraperitoneal [i.p.]). Data are representative of three independent experiments with three mice per genotype per treatment arm per experiment. Statistics were calculated using unpaired t test; mean ± SEM.

the spleen, we found that Nur77-GFP levels are not reduced but in fact are subtly higher in Anaef CD4$^+$ T cells compared with WT (Figure 1D). This suggests that Anaef T cells select for higher affinity TCRs, which compensates for the reduced GFP expression in developing thymocytes. The compensation in Nur77-GFP expression in peripheral T cells is not seen when the TCR repertoire is fixed so that all T cells bear the same receptor with identical affinity for antigen. In the context of the OTII TCR transgene, the magnitude of decrease in Nur77-GFP expression levels was even lower in Anaef thymocytes than in a polyclonal context, and splenic *Rasgrp1*^{Anaef} T cells also exhibited reduced Nur77-GFP levels compared with WT (Figures 1E and 1F). It is formally possible that this difference in Nur77-GFP signal is due to differences in expression of intracellular signaling molecules, though the RNA sequencing data in Figure 7 argue against this interpretation. Overall, in agreement with the T cell-dependent ANA and class-switching features, the T cells in the Anaef mice display a compensation for Nur77-GFP levels that suggest an altered, high-affinity TCR repertoire.

We previously reported that an increased proportion of Anaef T cells express PD-1 and Helios, markers for a follicular helper T cell (Tfh)-like population (Daley et al., 2013), but we never characterized these cells in greater detail. Here we found that Anaef CD4$^+$CD25$^-$ T cells in the spleen expressed higher levels of PD-1 and ICOS (Figure 1G), markers typically expressed on activated, but not resting, T cells (Wikenheiser and Stumhofer, 2016). The increased PD-1 and ICOS levels further increased with age of the Anaef mice (Figure 1H). CXCR5 and Bcl6 expression were more mildly increased on Anaef CD4$^+$ T cells (Figure 1G). This pattern of PD-1^{high}ICOS^{high}CXCR5^{low}Bcl6^{low} expression on Anaef CD4$^+$ T cells is reminiscent of a recently described T peripheral helper (Tph) cell subset that is expanded in joints of rheumatoid arthritis patients (Rao et al., 2017). Thus, Anaef mice display features of activated T cells and helper T cell-dependent immunopathology. We were interested in more fully characterizing the aberrant peripheral helper T cell populations in the Anaef model.

Peyer's patches (PPs) represent a natural anatomical site for germinal centers, where Tfh cells reside and provide help for B cell affinity maturation and isotype switching. Tfh cell differentiation is known to be affected by mTOR signaling (Yang et al., 2016; Zeng et al., 2016). Given that the *Anaef* allele increases tonic mTORC1 signals, we examined the PPs in unimmunized WT and Anaef mice. We found that Anaef mice have increased percentages of PD1^{hi}CXCR5^{hi} Tfh cells in the PPs (Figure 1I). This population expands in an mTORC1-dependent manner, as treating mice with rapamycin *in vivo* reduced the percentage of Tfh in the PPs compared with vehicle treatment (Figure 1J). Rapamycin also decreases the percentage of Tfh cells in WT mice (Figure S1B), indicating that tonic mTORC1 signaling promotes Tfh under normal homeostasis.

Tonic Signals in CD4 T Cells Preferentially Couple to the mTORC1 Pathway

Tonic TCR signals lead to low-level phosphorylation of proximal signaling molecules such as TCRζ (Stefanová et al., 2002) and Lck (Zikherman et al., 2010) in CD4$^+$ T cells isolated from lymph node (LN), but this basal phosphorylation is not observed in CD4$^+$ T cells from blood, where TCR contact with self-p-MHC is limited (Figure 2A). These tonic signals are dynamically maintained *in vivo*, as resting cells maintained *ex vivo* under non-stimulatory conditions reduce global basal tyrosine phosphorylation as well as phosphorylation of specific targets such as TCRζ (Daley et al., 2013; Myers et al., 2017a; Stefanová et al., 2002). Whereas the tonic signals proximal to the TCR have been well documented (Fulton et al., 2015; Hogquist et al., 2003; Mandl et al., 2013; Markegard et al., 2011; Stefanová et al., 2002; van Oers et al., 1993, 1994; Zikherman et al., 2010), it is largely unknown whether and how these proximal tonic signals connect to downstream effectors kinase pathways such as Ras-Erk, mTORC1-S6, and mTORC2-Akt (Figure 2B).

To determine the low-level activity in resting primary cells in a robust and quantitative manner, we coupled fluorescent cellular barcoding to phospho-flow cytometry on freshly isolated cells from LNs so that staining with antibodies to phosphorylated proteins is internally controlled (Krutzik and Nolan, 2006; Ksionda et al., 2018) (Figure 2C). Using this platform, we observed a strikingly robust P-S6 signal in CD4$^+$ T cells (roughly 12-fold over background) when LN cells were fixed immediately upon dissection (Figure 2D). Note that we used P-S6$^{S235/236}$ as readout of mTORC1 activity because expression levels of the 4EBP proteins, canonical mTORC1 substrates, are very low in naive CD4$^+$ T cells (data not shown). This P-S6$^{S235/236}$ signal dissipates to nearly background levels if cells are rested at low density to limit cell-cell contact in medium containing glucose and amino acids but without serum (Figure 2D). By contrast, Ras-Erk and mTORC2-Akt signals appear to be much less tonically active; P-Akt^{S473} signals (mTORC2 activity) only modestly decreased with a 2 h rest, and P-Erk$^{T202/Y204}$ (Ras activity) did not decrease in this time frame (Figure 2D; Figure S2A). Freshly isolated and fixed CD4$^+$ T cells from blood, where interactions with self-p-MHC are limited, demonstrated little mTORC1-S6 signal compared with CD4$^+$ T cells from LN (Figure 2E), in agreement with the model in Figure 2A. CD44 is a cell surface marker reported to be a translational target of mTORC1 signaling in prostate cancer cells (Hsieh et al., 2012) and CD4$^+$ T cells (Daley et al., 2013). Treatment of mice *in vivo* with a low dose of rapamycin for 1 week (Daley et al., 2013) resulted in reduced levels of CD44 on naive CD4$^+$ T cells (Figure 2F), demonstrating that tonic mTORC1 signals occur in T cells *in vivo* and affect CD44 expression levels.

Rasgrp1 Signals to mTORC1 in a Tonic Fashion

Rasgrp1 exists as an autoinhibited dimer in the basal state, but autoinhibition is not absolute (Iwig et al., 2013), and we postulated that Rasgrp1 could signal to mTORC1 in lymphocytes in a tonic manner. Data supporting this can be found in a study in which unstimulated *Rasgrp1*-deficient thymocytes were analyzed as a control (Gorentla et al., 2011). To test our hypothesis, we first used a DT40 chicken B cell line with genetic deletion of all *Rasgrp1* and *Rasgrp3* alleles (double knockout [DKO]), which we used previously (Das et al., 2009). In the absence of any stimulation, WT DT40 cells exhibited robust basal phosphorylation of S6, whereas P-S6 is reduced in DKO cells (Figure 3A). Transient reconstitution of DKO cells with WT Rasgrp1-EGFP was sufficient to rescue the tonic P-S6 defect in a Rasgrp1

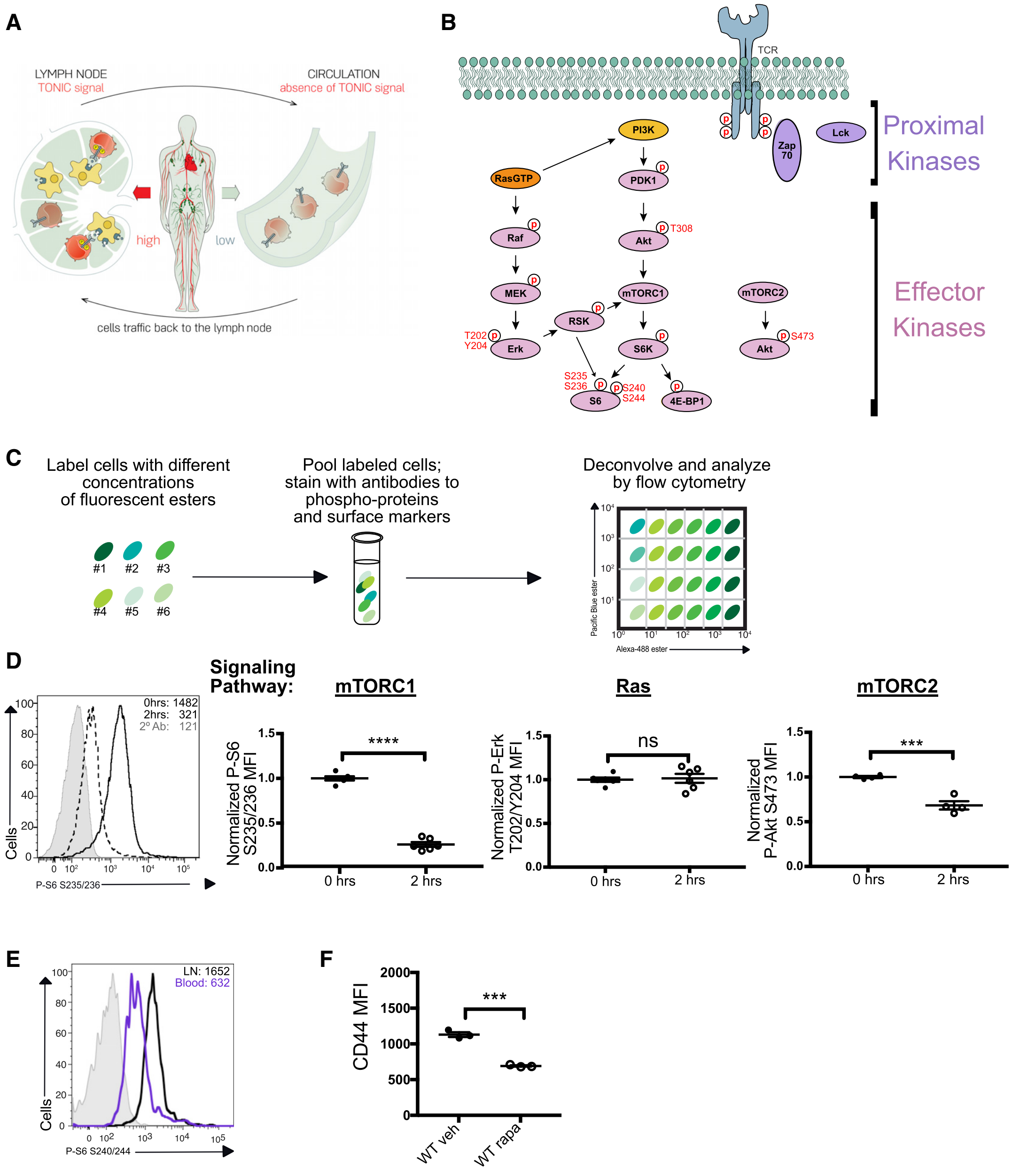

Figure 2. Tonic Signals in CD4 T Cells Preferentially Couple to the mTORC1 Pathway

(A) Schematic summarizing level of tonic signaling in lymphocytes in different anatomical locations.

(B) Schematic of signaling pathways proximal to the TCR and downstream effector kinase pathways, including mTORC1-S6K-S6, Ras-Erk, and mTORC2-Akt.

(C) Schematic of fluorescent cellular barcoding technique used in phospho-flow assays. Cells from individual mice or tissues are labeled with different concentrations of fluorescent succinimidyl esters, pooled, and stained for markers of interest. The pool is run on a flow cytometer, and data are deconvolved so signaling in each population can be analyzed.

(D) Phospho-flow cytometry on lymph node cells from WT mice immediately fixed upon dissection or rested for 2 h prior to fixation. Fixed cells were barcoded as in (C) and stained with antibodies to CD4 and the indicated phospho-proteins. Background (gray histogram) is cells stained with secondary antibody without primary antibody. Statistical significance was calculated using an unpaired t test, and error bars represent SEM. Data are representative of two to six independent experiments. Statistics were calculated using unpaired t test; mean ± SEM.

(E) Phospho-flow cytometry on lymph node and blood cells from WT mice immediately fixed upon dissection. Cells from individual tissues were barcoded as in (C) and stained with antibodies to CD4 and P-S6$^{S240/244}$. Gray histogram is background, as in (D). Data are representative of four independent experiments with three to five mice per experiment.

(F) Flow cytometric analysis of CD44 levels on naive CD4^{+} T cells from 12-week-old WT mice treated for 1 week with vehicle or rapamycin (0.4 mg/kg, i.p.). CD44 MFI was calculated for TCRβ^{+} CD4^{+} CD62L^{hi} naive T cells, and statistics were calculated using unpaired t test; mean ± SEM. Data are representative of three independent experiments with three mice per genotype per treatment arm per experiment.

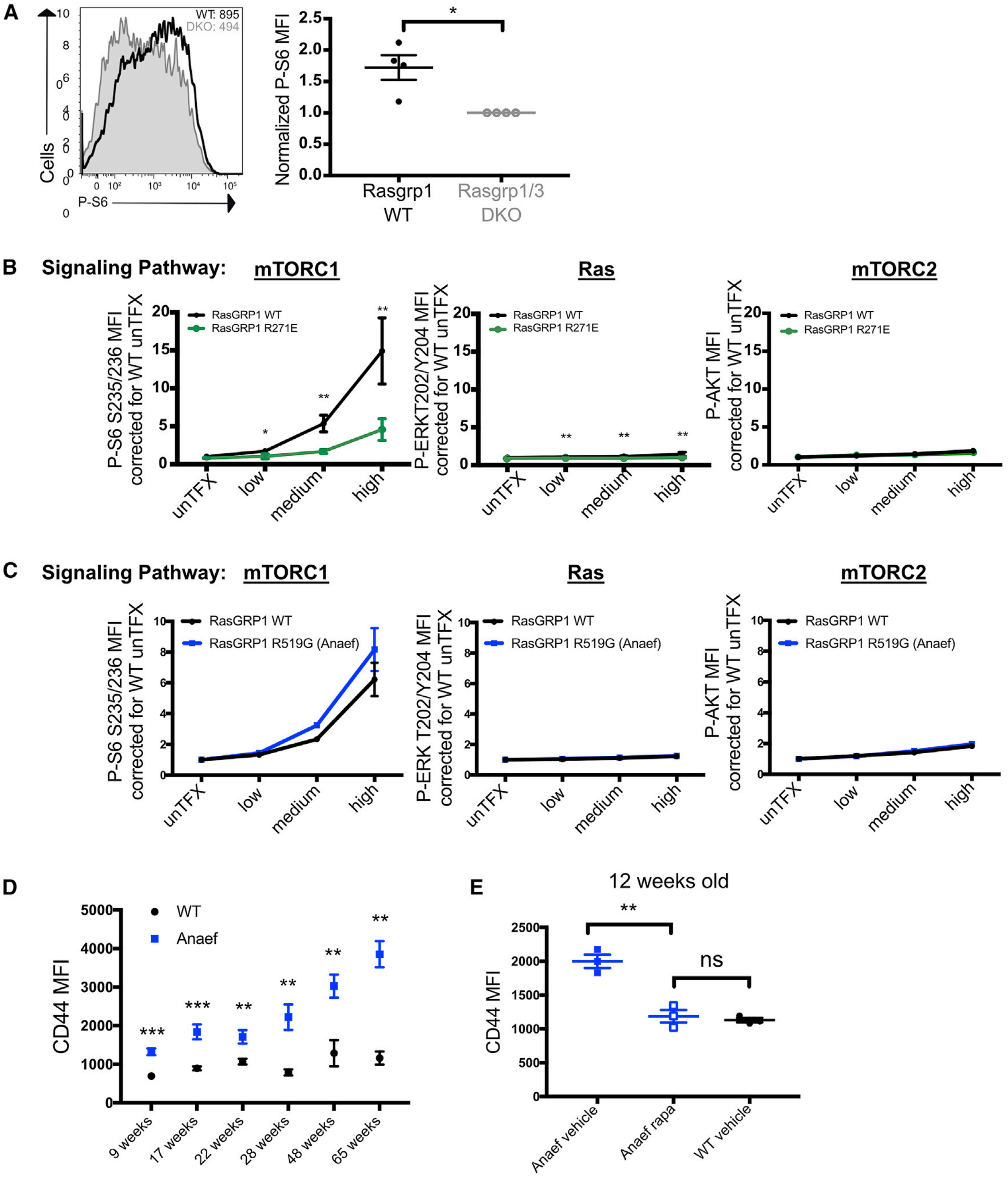

Figure 3. Rasgrp1 Signals to mTORC1 in a Tonic Fashion

(A) Phospho-flow cytometry on WT and Rasgrp1$^{-/-}$ Rasgrp3$^{-/-}$ (DKO) DT40 cells immediately fixed from culture. Histogram is representative of three independent experiments. Data were normalized and pooled by setting the DKO MFI from each experiment to 1, and statistical significance was calculated using an unpaired t test.

(B) Phospho-flow cytometry on DKO DT40 cells transiently transfected with Rasgrp1^{WT}-EGFP or Rasgrp1^{R271E}-EGFP constructs. Cells were gated on the basis of level of GFP (low, medium, or high) prior to analyzing phosphorylation, and statistical significance was calculated using an unpaired t test. Data are representative of four to six independent experiments.

(C) As in (B) but transfection with Rasgrp1^{WT}-EGFP or Rasgrp1^{R519G}-EGFP constructs. Data are representative of four to six independent experiments.

(D) Flow cytometric analysis of CD44 levels (MFI) on CD4$^+$ CD25$^-$ splenic T cells from WT and Anaef mice at the indicated ages. Statistical significance determined using the Holm-Sidak method, with alpha = 0.05. Data are from one experiment with two to six mice per genotype per age.

(E) Flow cytometric analysis of CD44 levels on naive CD4$^+$ T cells from 12-week-old WT and Anaef mice treated for 1 week with vehicle or rapamycin (0.4 mg/kg, i.p.). CD44 MFI was calculated for TCRb$^+$ CD4$^+$ CD62L^{hi} cells, and statistics were calculated using unpaired t test; mean ± SEM. Data are representative of three independent experiments with three mice per genotype per treatment arm per experiment.

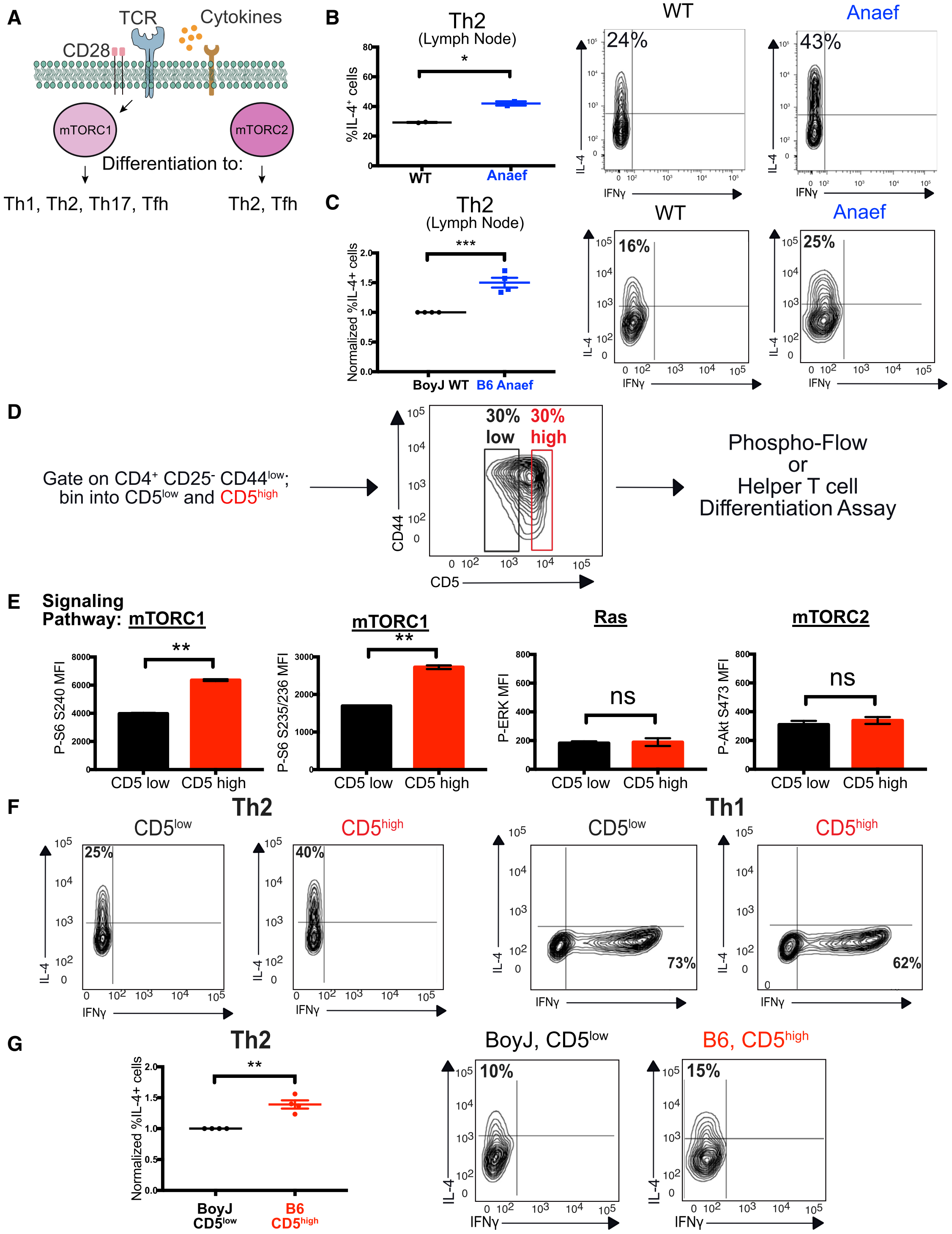

Figure 4. Cells with High Tonic mTORC1 Signaling Exhibit Increased Th2 Differentiation

(A) Schematic of mTORC1 and mTORC2 in T cells. Multiple upstream inputs can activate these kinases, and they have been demonstrated to affect differentiation to distinct effector T cell lineages.

(B) *In vitro* Th2 differentiation assay with WT and Anaef lymph node CD4$^+$ T cells. Data are representative of six independent experiments with two to four mice per group; statistics were calculated using unpaired t test; mean ± SEM.

(C) As in (B), but equal numbers of WT BoyJ (CD45.1) and Anaef B6 (CD45.2) cells were co-cultured in Th2 conditions. Contour plots are representative of two independent experiments with two mice per group. Data from individual experiments were normalized to the WT cells within that experiment, pooled, and statistical significance was calculated using an unpaired t test.

(legend continued on next page)

dose-dependent manner (Figure 3B). Rasgrp1 catalytic activity is required, as we observed very little rescue of P-S6$^{S235/236}$ in cells transfected with a catalytically inactive Rasgrp1^{R271E}, even in cells with highest Rasgrp1 expression (Figure 3B). Rasgrp1 induced a modest increase in basal Ras-Erk signals but did not affect mTORC2-Akt signals (Figure 3B). The Rasgrp1 signal to S6 could be blocked with the mTORC1 inhibitor rapamycin but not with the Rsk inhibitor BI-D1870 (Figure S2B), indicating that the P-S6 signal was due to Rasgrp1-mTORC1-S6K-S6 signaling and not an Erk-Rsk-S6 pathway (Roux et al., 2007).

Transfection of DT40 DKO cells with a Rasgrp1^{R519G}-EGFP construct revealed that the *Rasgrp1^{Anaef}* allele is moderately hypermorphic in its basal signaling capacity to P-S6$^{S235/236}$ (Figure 3C) but not to Ras-ERK or mTORC2-Akt (Figure 3C). *Rasgrp1^{Anaef}* mice exhibit autoimmune features (Figure 1B), and we demonstrated that crossing these mice to a hypomorphic mTOR allele corrects these features (Daley et al., 2013). When we analyzed CD44 expression levels on CD4^{+} T cells as a function of age, we noted that CD44 levels continued to rise on Anaef T cells (Figure 3D), illustrating the cumulative effects of elevated tonic mTORC1 signals over time. Treating a cohort of Anaef mice with a low dose of rapamycin *in vivo* restored the elevated expression levels of the mTORC1 target CD44 on CD4^{+} LN T cells to WT levels (Figure 3E).

Cells with High Tonic mTORC1 Signaling Exhibit Increased Th2 Differentiation

Given that Tfh cells accumulate in naive Rasgrp1^{Anaef} mice in an mTORC1-dependent manner and that Rasgrp1^{Anaef} mice exhibit other immunopathology, we were interested in determining what other helper T cell features were affected by Anaef-mTORC1 tonic signals. Most studies to date have analyzed TCR-induced mTOR signaling and have relied on genetic perturbation. Genetically deleting mTOR complex components in mice alters T cell differentiation driven by TCR and cytokine stimulation (summarized in Figure 4A). Deletion of Rheb (Delgoffe et al., 2011) or Raptor (Yang et al., 2013) revealed requirements for mTORC1 signals in Th1, Th2, and Th17 differentiation, whereas deletion of Rictor to abrogate mTORC2 signaling reduced the ability to generate Th2 cells (Delgoffe et al., 2011; Yang et al., 2013). Loss of mTOR does not affect differentiation to the regulatory T cell (Treg) lineage (Delgoffe et al., 2009), but Raptor deletion in FoxP3^{+} Treg cells revealed that mTORC1 is required for suppressive capacity *in vivo* (Zeng et al., 2013). Last, both mTORC1 and mTORC2 are required for generation of Tfh (Yang et al., 2016; Zeng et al., 2016).

In contrast, the Anaef model provided an unique opportunity to investigate how tonic mTORC1 signals in T cells *in vivo* may affect the potential of naive T cells to differentiate into effector T cell subsets when stimulated *in vitro*. Importantly, the Anaef model allows this assessment without perturbing the mTOR complexes through genetic deletion. We performed *in vitro* differentiation assays with WT and Anaef CD4^{+} cells. Interestingly, Anaef CD4^{+} T cells displayed enhanced ability to differentiate into Th2 cells and produce interleukin (IL)-4 (Figure 4B). This phenotype was cell intrinsic, as we observed enhanced Th2 differentiation when congenically marked WT and Anaef cells were co-cultured and differentiated in the same well (Figure 4C). The differentiation phenotype was specific to Th2, as Anaef and WT cells were equally fit to generate inferno (IFN)γ-producing Th1 cells as well as IL-17-producing Th17 cells and FoxP3^{+}/CD25^{+} iTreg cells (Figure S3). In sum, these data demonstrate that increased tonic Anaef-mTORC1 signals enhance the potential to differentiate to the Th2 fate. The data imply that levels of tonic mTORC1 signals prime the basal state of CD4^{+} T cells, a feature we further investigated functionally and mechanistically.

CD5 has been used as a marker of tonic proximal TCR signaling in thymocytes and T cells (Azzam et al., 1998; Fulton et al., 2015; Mandl et al., 2013). We used CD5 to examine tonic mTORC1 signals in WT naive CD4^{+} T cells, extending our findings beyond the Anaef model. First, to determine whether mTORC1 signaling is also selectively robust in the heterogeneous WT T cell pool, we immediately fixed LN cells and performed phospho-flow cytometry to analyze basal signaling in naive (CD25^{-} CD44^{low}) CD4^{+} T cells gated into populations with the 30% highest and 30% lowest CD5 expression (Figure 4D). CD5^{high} cells exhibited increased P-S6$^{S240/244}$ and P-S6$^{S235/236}$ compared with the 30% lowest CD5 expressing cells (Figure 4E). In agreement with our findings that Ras-Erk and mTORC2-Akt pathways do not appear tonically active (Figure 2D; Figure S2A), we did not observe differences in P-Erk$^{T202/Y204}$ or P-Akt^{S473} in cells with different CD5 levels (Figure 4E). This is consistent with an independent study, which also showed that levels of tonic P-Erk$^{T202/Y204}$ did not change as a function of CD5 level (Persaud et al., 2014).

We next set out to test whether the level of tonic signal a WT cell receives affects its differentiation into effector subsets. In Th2 polarizing assays, sorted, naive CD4^{+}CD5^{high} cells (highest tonic signaling) yielded more IL-4-producing Th2 cells than CD4^{+}CD5^{low} counterparts from the same sort (Figure 4F). In Th1 polarizing conditions, we found that cells with CD5^{high} cells differentiated slightly less robustly into IFNγ-producing Th1 cells compared with CD5^{low} cells (Figure 4F). The increased fitness of naive CD4^{+}CD5^{high} cells to polarize to Th2 was cell intrinsic (Figure 4G). In sum, the CD5 platform validates the finding that tonic

---

(D) Schematic of gating scheme for phospho-flow cytometry shown in (E) and cell-sorting strategy used as input for assays in (F) and (G).

(E) Phospho-flow cytometry on WT lymph node cells immediately fixed upon dissection. Cells were barcoded, stained, and gated as indicated in (D) prior to analysis of phospho-markers. Statistical significance was calculated using an unpaired t test. Data are representative of four independent experiments with three mice per experiment.

(F) *In vitro* Th1 and Th2 differentiation assay on sorted CD5^{low} and CD5^{high} CD4^{+} T cells. Data are representative of six independent experiments with two mice per experiment.

(G) As in (F) but equal numbers of sorted WT CD5^{low} BoyJ (CD45.1) and WT CD5^{high} B6 (CD45.2) cells were co-cultured in Th2 conditions. Contour plot is representative of two independent experiments with two mice per group, and graph is normalized and pooled data from both experiments. Statistical significance was calculated using an unpaired t test.

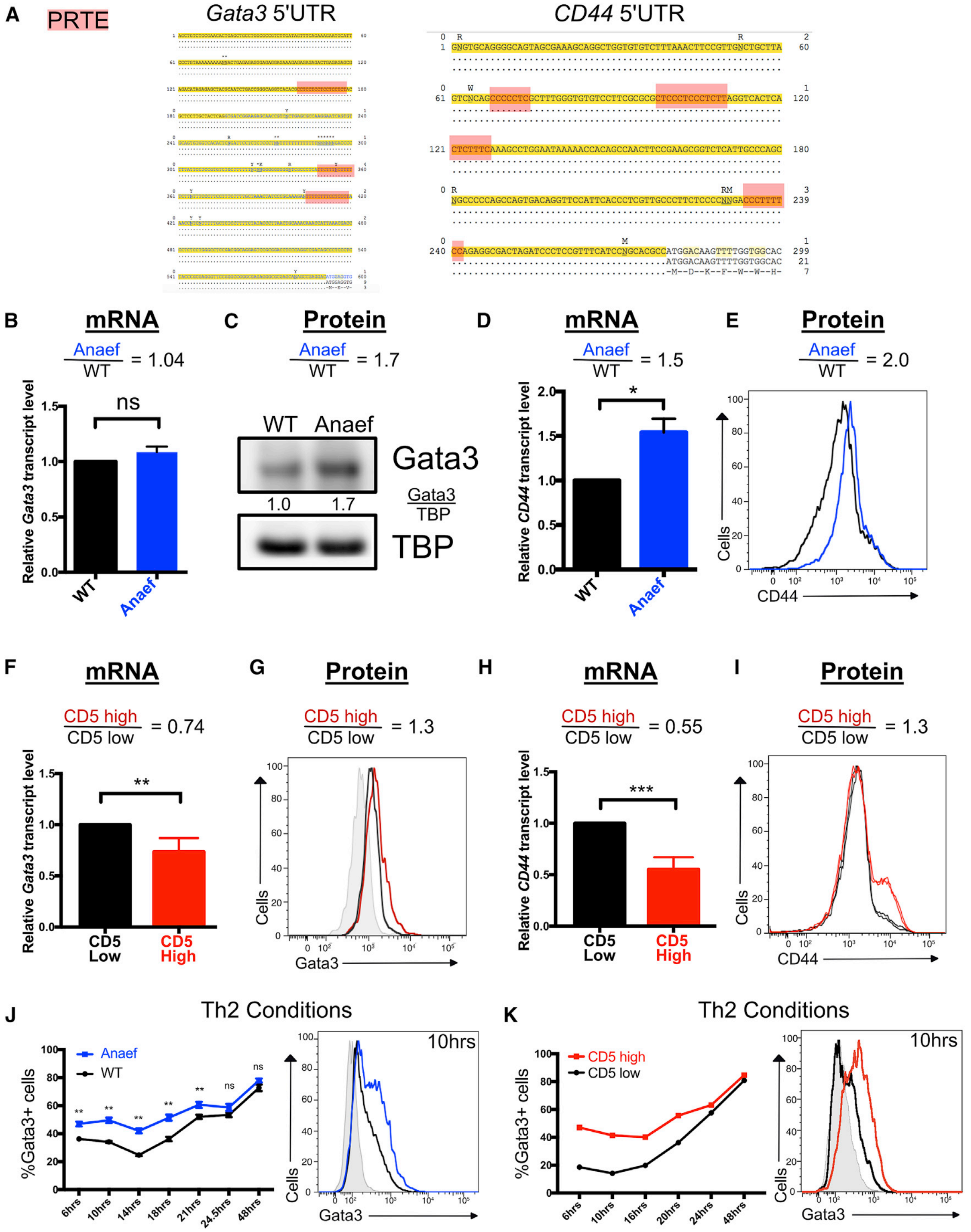

Figure 5. Tonic mTORC1 Signaling and Translation of Target Genes in Naive CD4$^+$ T Cells

(A) Identification of pyrimidine-rich translational elements (PRTEs) in the 5′ UTRs of murine *Gata3* and *CD44*. Sequences were obtained from Ensembl.

(B) TaqMan analysis of basal *Gata3* mRNA levels in WT and Anaef CD4$^+$ T cells. *Gata3* levels were normalized to the housekeeping gene *Ppia*. Statistical significance was calculated using an unpaired t test. Data are from four independent T cell purifications with n = 3 technical replicates per sample.

(C) Immunoblotting for Gata3 and TBP (loading control) in purified CD4$^+$ T cells from WT and Anaef mice. Data are representative of three independent experiments.

(D) TaqMan analysis of basal *CD44* mRNA levels in WT and Anaef CD4$^+$ T cells. *CD44* levels were normalized to the housekeeping gene *Ppia*. Statistical significance was calculated using an unpaired t test. Data are from four independent T cell purifications, with n = 3 technical replicates per sample.

(E) Flow-cytometric analysis of CD44 protein levels (MFI) on WT and Anaef CD4$^+$ T cells from the same animals as in (D).

(legend continued on next page)

mTORC1 signals are uniquely robust in naive CD4$^+$ T cells and prime the efficiency of Th2 differentiation.

Tonic mTORC1 Signaling and Translation of Target Genes in Naive CD4$^+$ T Cells

We next sought to understand how mechanistically tonic mTORC1 signals affect naive T cell differentiation into specialized subsets. We hypothesized that translation may be regulated in a tonic manner in naive T cells, because mTOR is known to be a key regulator of mRNA translation (Araki et al., 2017; Chi, 2012; Powell et al., 2012; Tan et al., 2017; Waickman and Powell, 2012). Translational targets of mTOR often contain specific sequence elements in their 5′ UTR, such as a 5′ terminal oligopyrimidine tract (5′TOP) or a pyrimidine-rich translational element (PRTE) (Gentilella and Thomas, 2012; Hsieh et al., 2012; Thoreen et al., 2012). A prostate cancer cell screen demonstrated that 89% of mTOR target mRNAs have either a 5′TOP or a PRTE, and 63% of these have only a PRTE (Hsieh et al., 2012).

The transcription factor Gata3, the cytokine IL-4, and the costimulatory molecule ICOS are examples of Th2- and Tfh-relevant genes that are regulated at the translational level (Cook and Miller, 2010; Gigoux et al., 2014; Piccirillo et al., 2014; Scheu et al., 2006). Gata3 is critical for Th2 differentiation (O'Shea and Paul, 2010) and plays a role in Tfh biology (Liu et al., 2013). We found that the mouse *Gata3* 5′UTR contains PRTEs (Figure 5A). Consistent with the findings that CD44 levels on Anaef CD4$^+$ T cells rise over time (Figure 3D) and that rapamycin reduces CD44 levels on CD4$^+$ T cells (Figures 3E), we also detected PRTEs in the 5′UTR of murine *CD44* (Figure 5A). The human prostate cancer cell study revealed both a 5′TOP and PRTE in human *CD44* (Hsieh et al., 2012).

We next compared *Gata3* and *CD44* mRNA levels using qPCR and their protein levels using barcoding flow cytometry and immunoblot. In these comparisons, we analyzed both CD4$^+$ T cells from Anaef compared with WT mice (Figures 5B–5E) and WT CD4$^+$ T cells subsetted into CD5^{high} and CD5^{low} (Figures 5F–5I). These independent platforms revealed that *Gata3* and *CD44* are under tonic translational control. Although the fold increase in translation of *Gata3* and *CD44* in Anaef or CD5^{high} CD4$^+$ T cells may seem modest, one must keep in mind that tonic signaling is constantly occurring and thus can lead to cumulative increases in protein levels over time, as demonstrated in Figures 1H and 3D.

Increased percentages of Anaef CD4$^+$ T cells (compared with WT) and WT CD5^{high} cells (compared with CD5^{low}) expressed Gata3 early on during initiation of the Th2 fate and sustain Gata3 during the first 24 h of culture (Figures 5J and 5K). Our results reveal that cells with high tonic signaling and elevated Gata3 are biased toward Th2 lineage commitment, which fits with Gata3 as an auto-amplifying Th2 master switch (Ouyang et al., 2000) as well as with a well-accepted IL4-Gata3-IL4 positive feedback loop during Th2 differentiation (Ansel et al., 2006; Paul, 2010).

The Translational Profile of Naive CD4 T Cells Reveals an mTOR Signature

To examine tonic translational control at a genome-wide level, we used ribosome profiling, a method in which ribosome-protected fragments (RPFs) are isolated and subjected to high-throughput sequencing. The RPF sequences are compared with total mRNA in the cells to calculate translation efficiency (Brar and Weissman, 2015; Ingolia et al., 2013). Translation occurs at a low level in CD4$^+$ T cells of unimmunized mice (Araki et al., 2017; Bjur et al., 2013; Tan et al., 2017). We performed ribosome profiling and total mRNA sequencing on a >97% pure population of CD4$^+$CD25$^-$ T cells isolated from LN of 12-week-old, healthy, unimmunized WT mice. In parallel, we analyzed 12-week-old unimmunized Anaef mice, an age when changes in CD44 expression and ANAs only just start to appear (Figure 6A; Figure S4A).

Ribosome profiling with a focus on mTOR has been performed on proliferating cells (Hsieh et al., 2012; Thoreen et al., 2012) but is uncommon for resting cells, and as such we first ran a number of quality controls. In order to obtain sufficient material for sequencing, LNs were pooled from mice with the same genotype (Figure 6A). In total we obtained 50 million to 67 million reads from each WT RPF biological replicate and approximately 40 million reads from each Anaef replicate. We removed rRNA reads (roughly 43%–55% of reads per sample), discarded reads that map to multiple places in the genome, and masked reads that mapped to the first or last five codons. Keeping only annotated transcript-mapping reads, we used 2.9 million to 7.0 million reads per sample for further analysis. We observed that the majority of ribosome-protected fragment (RPF) lengths were between 27 and 31 nt, consistent with the size of a standard RPF (Brar and Weissman, 2015; Ingolia et al., 2013; Figure S4B). As expected, the majority of RPF reads mapped to the 5′ end of genes relative to the coding sequence, and very few reads mapped to the 3′UTR (Figures S4C and S4D). In contrast, total RNA sequencing (RNA-seq) reads mapped throughout the

---

(F) TaqMan analysis of basal Gata3 mRNA levels in sorted WT CD4$^+$ CD25$^-$ CD44^{low} CD5^{low} and CD5^{high} cells. *Gata3* levels were normalized to the housekeeping gene *Ppia*. Statistical significance was calculated using an unpaired t test. Data are from five independent sorts with n = 3 technical replicates per sample.

(G) Flow-cytometric analysis of Gata3 protein levels (MFI) on WT CD4$^+$ CD25$^-$ CD44^{low} CD5^{low} and CD5^{high} cells from the same animals as (F). Gray-shaded histogram is an isotype control. Data are from three independent experiments.

(H) TaqMan analysis of basal *CD44* mRNA levels in sorted WT CD4$^+$ CD25$^-$ CD44^{low} CD5^{low} and CD5^{high} cells. *CD44* levels were normalized to the housekeeping gene *Ppia*. Statistical significance was calculated using an unpaired t test. Data are from five independent sorts, with n = 3 technical replicates per sample.

(I) Flow-cytometric analysis of CD44 protein levels (MFI) on sorted WT CD4$^+$ CD25$^-$ CD44^{low} CD5^{low} and CD5^{high} cells from the same animals as (H).

(J) Flow cytometric analysis of Gata3 levels in WT and Anaef CD4$^+$ T cells fixed at the indicated time points in Th2 differentiation conditions. Histogram for the 10 h time points is highlighted. Gray-shaded histogram represents isotype control. Statistical significance determined using the Holm-Sidak method, with alpha = 0.05. Data are representative of four independent experiments with two or three mice per group.

(K) Flow cytometric analysis of Gata3 levels in WT CD4$^+$ CD25$^-$ CD44^{low} CD5^{low} and CD5^{high} cells fixed at the indicated time points in Th2 differentiation conditions. Histogram for the 10 h time points is highlighted. Gray-shaded histogram represents isotype control. Data are representative of two independent experiments.

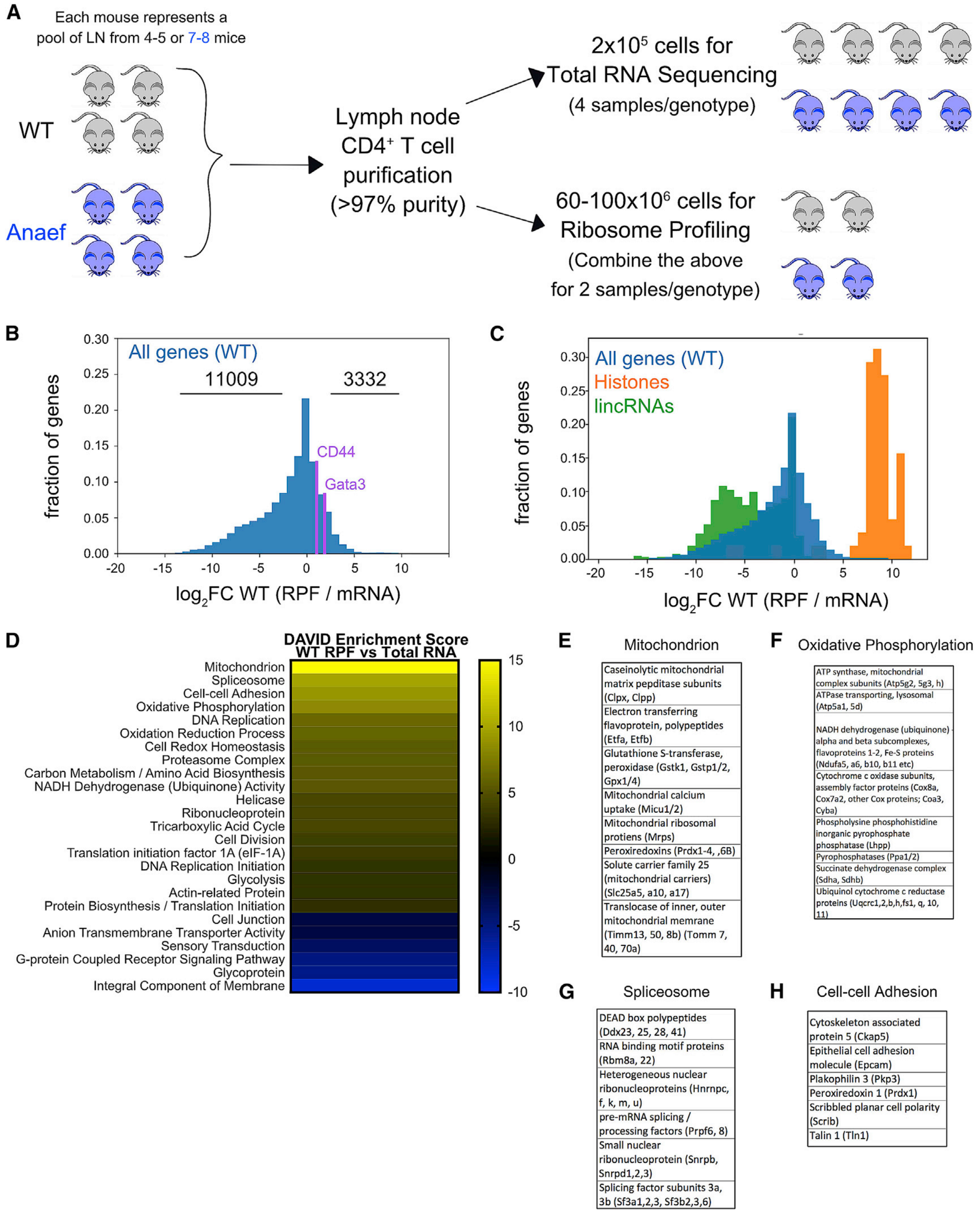

E Mitochondrion

Caseinolytic mitochondrial matrix pepditase subunits (Clpx, Clpp)
Electron transferring flavoprotein, polypeptides (Etfa, Etfb)
Glutathione S-transferase, peroxidase (Gstk1, Gstp1/2, Gpx1/4)
Mitochondrial calcium uptake (Micu1/2)
Mitochondrial ribosomal protiens (Mrps)
Peroxiredoxins (Prdx1-4, ,6B)
Solute carrier family 25 (mitochondrial carriers) (Slc25a5, a10, a17)
Translocase of inner, outer mitochondrial memrane (Timm13, 50, 8b) (Tomm 7, 40, 70a)

F Oxidative Phosphorylation

ATP synthase, mitochondrial complex subunits (Atp5g2, 5g3, h)
ATPase transporting, lysosomal (Atp5a1, 5d)
NADH dehydrogenase (ubiquinone) alpha and beta subcomplexes, flavoproteins 1-2, Fe-S proteins (Ndufa5, a6, b10, b11 etc)
Cytochrome c oxidase subunits, assembly factor proteins (Cox8a, Cox7a2, other Cox proteins; Coa3, Cyba)
Phospholysine phosphohistidine inorganic pyrophosphate phosphatase (Lhpp)
Pyrophosphatases (Ppa1/2)
Succinate dehydrogenase complex (Sdha, Sdhb)
Ubiquinol cytochrome c reductase proteins (Uqcrc1,2,b,h,fs1, q, 10, 11)

G Spliceosome

DEAD box polypeptides (Ddx23, 25, 28, 41)
RNA binding motif proteins (Rbm8a, 22)
Heterogeneous nuclear ribonucleoproteins (Hnrnpc, f, k, m, u)
pre-mRNA splicing / processing factors (Prpf6, 8)
Small nuclear ribonucleoprotein (Snrpb, Snrpd1,2,3)
Splicing factor subunits 3a, 3b (Sf3a1,2,3, Sf3b2,3,6)

H Cell-cell Adhesion

Cytoskeleton associated protein 5 (Ckap5)
Epithelial cell adhesion molecule (Epcam)
Plakophilin 3 (Pkp3)
Peroxiredoxin 1 (Prdx1)
Scribbled planar cell polarity (Scrib)
Talin 1 (Tln1)

Figure 6. The Translational Profile of Naive CD4 T Cells Reveals a mTOR Signature

(A) Schematic of the experimental design for paired ribosome profiling and total mRNA sequencing. Lymph nodes from individual mice were pooled across four WT and four Anaef samples, and CD4$^+$ CD25$^-$ T cells were purified. Twenty thousand cells were lysed, and total mRNA was extracted using oligo-dT hybridization, which was used for RNA-seq library preparation and sequencing. The remaining biologicals replicates were pooled to give two WT and two Anaef samples of 60 × 10^6 to 100 × 10^6 cells, which were lysed for ribosome profiling library preparation and sequencing.

(B) Histogram plot of DESeq2-calculated $\log_2$ fold change ($\log_2$FC) of ribosome-protected fragment (RPF) reads relative to total RNA. The number of genes that had a $\log_2$FC greater than 1 are indicated, and the $\log_2$FC values of CD44 and Gata3 are indicated by purple lines.

(C) As in (B), but with histone genes overlaid as an orange histogram and lincRNAs as a green histogram (a list of lincRNAs was obtained from Ensembl).

(D) Heatmap of the pathways enriched in the 3,000 most differentially expressed genes (up and down) in the WT RPF compared with WT total RNA. Functional annotation clustering was performed, and enrichment scores were calculated using DAVID, with the entire WT RPF versus Total RNA DESeq2 dataset used as background.

(legend continued on next page)

transcripts, including the 5′ and 3′UTRs (Figures S4C and S4D). Thus, this approach worked technically, yet we did note that the purity for WT $CD4^+CD25^-$ T cells was slightly lower than for Anaef cells (Figure S4A).

To determine how many targets were preferentially bound by ribosomes in resting WT $CD4^+$ T cells, we performed differential expression analysis using DESeq2, comparing our RPF and total RNA datasets from WT mice. A total of 3,332 genes were significantly enriched 2-fold or more in RPFs relative to mRNA, whereas 11,009 genes were more significantly enriched 2-fold or more in the mRNA relative to the RPF (Figure 6B). The small number of genes differentially bound to ribosomes is consistent with relatively low translation in resting T cells (Araki et al., 2017; Bjur et al., 2013; Tan et al., 2017). Histone genes, which are not polyadenylated (Marzluff et al., 2008) and thus would not be included in our total RNA-seq as we purified total RNA by oligo-deoxythymine (oligo-dT) hybridization, were highly enriched in our RPF data (Figure 6C, orange histogram). In contrast, long intergenic noncoding RNAs (lincRNAs; Ensembl mouse dataset), which are not translated (Guttman et al., 2013), were more enriched in the total mRNA fraction (Figure 6C, green histogram). Thus, there is a translational landscape in resting $CD4^+$ T cells. To obtain an initial impression of the types of targets in the 3,332 genes, we compared these with a published list of mTOR target genes from proliferating P53-deficient MEFs treated with the mTOR inhibitor Torin 1 (Thoreen et al., 2012). Of the 232 Torin-sensitive genes in MEFs (Thoreen et al., 2012), 128 also appeared in our WT $CD4^+$ T cell RPF dataset. *Gata3* and *CD44*, genes we identified as translational targets of mTOR in T cells (Figure 5), were also enriched in the RPF dataset relative to total RNA (Figure 6B).

We subsequently took a more unbiased approach to understand the types of target genes that were bound by ribosomes in the basal state. We used the Database for Annotation, Visualization and Integrated Discovery (DAVID; version 6.8) to perform functional annotation clustering on the 3,000 most upregulated and 3,000 most downregulated genes in our WT dataset. Enrichment scores are listed as positive for pathways that were overrepresented in the RPF fraction and negative for pathways overrepresented in the mRNA. Remarkably, mitochondrial genes and genes involved in oxidative phosphorylation were among pathways enriched among mRNAs being translated (Figures 6D–6F). In agreement with our discovery of robust tonic mTORC1 signals in resting $CD4^+$ T cells, mTOR-regulated processes of translation and protein biogenesis were enriched in the RPF fraction (Figure 6D). Perhaps more unexpectedly, spliceosome and cell-cell adhesion were also in the top four functional annotation clusters (Figures 6G and 6H). RNA binding proteins, including splicing proteins, are typically regulated at the RNA level (such as through translation) (Fu and Ares, 2014; Martinez and Lynch, 2013). The spliceosome genes mostly encode core spliceosome proteins, and without these, splicing does not occur (Fu and Ares, 2014; Martinez and Lynch, 2013). CD44 is a migration receptor; CD44 binding to ligands such as the extracellular matrix component hyaluronic acid can affect T cell proliferation and cytokine production (Baaten et al., 2013). In sum, we established that there is a translational landscape in resting $CD4^+$ T cells that is rich in mTOR-regulated targets, as well as targets that affect processes such as mitochondrial metabolism and splicing.

Rasgrp1^Anaef CD4 T Cells Reveal Subtle Changes in Translational Landscape before Onset of Autoimmunity

Last, we aimed to understand how Anaef T cells might alter their cell biology and lineage fate before the onset of the described immunopathology. To do this, we examined $CD4^+$ T cells isolated from young (12-week-old) Anaef mice, and not from older (>28 weeks) mice, when autoimmunity is prevalent and Tph and Tfh cells have begun to accumulate (Figure 1). Comparison of the WT and Anaef total RNA datasets revealed that WT and Anaef $CD4^+$ cells are very similar at the transcriptional level, with a Pearson's correlation coefficient of 0.997 (Figure 7A). We noted that some B cell-specific transcripts appeared in some WT replicates (approximately 3% non-$CD3^+CD4^+$ cells; Figure S5A); given that these were contaminants, we excluded them from our analysis (Figure 7A; Figure S5A). Profiled ribosomes from Anaef $CD4^+$ T cells revealed that 3545 genes in resting Anaef $CD4^+$ T cells were enriched 2-fold or greater in the RPF dataset relative to Anaef total RNA (Figure 7B). Functional annotation of these genes (DAVID) demonstrated that resting $CD4^+$ T cells from 12-week-old Anaef mice also revealed a ribosome landscape enriched for targets that fall into mitochondria, spliceosome, oxidative metabolism, and translation initiation pathways, as seen for WT $CD4^+$ T cells (Figure 7C). In addition, chromatin remodeling and glutathione metabolism were enriched pathways unique to the Anaef dataset (Figure 7C). Glutathione functions as an antioxidant that controls oxidative stress (Mak et al., 2017; Meister, 1983). Together, these studies indicate a connection between mTOR, glutathione metabolism, and regulation of T cell responses.

Focusing on the specific translated target genes, the identity of the ribosome profiles between WT and Anaef resting $CD4^+$ T cells showed a high degree of similarity, with 2921 overlapping gene targets (Figure 7D), but also revealed a small subset of genes that were more highly enriched in Anaef $CD4^+$ T cells compared with WT (Figures 7D, 7E, and S5B). Thus, the Anaef translational landscape displayed unique features. Further interrogating the 624 uniquely translated genes in Anaef T cells (Figure 7D), we compared the $\log_2$ fold change (FC) of the RPF RPMs for each genotype and plotted these against the $\log_2$FC of the total RNA RPMs for each genotype to assess which target genes were affected at the translational versus transcriptional level (Figure 7E). Genes such as Stfa3 (*stefin A3*) were regulated at the level of translation, but some other genes, such as Gm10722, which mapped to un-annotated regions, are likely artifacts because of low reads per million in both Anaef replicates (Figure 7E). In sum, there are subtle alterations in the translational

---

(E) List of select genes from the mitochondrion cluster identified in (D).

(F) List of select genes from the oxidative phosphorylation cluster identified in (D).

(G) List of select genes from the spliceosome cluster identified in (D).

(H) List of select genes from the cell-cell adhesion cluster identified in (D).

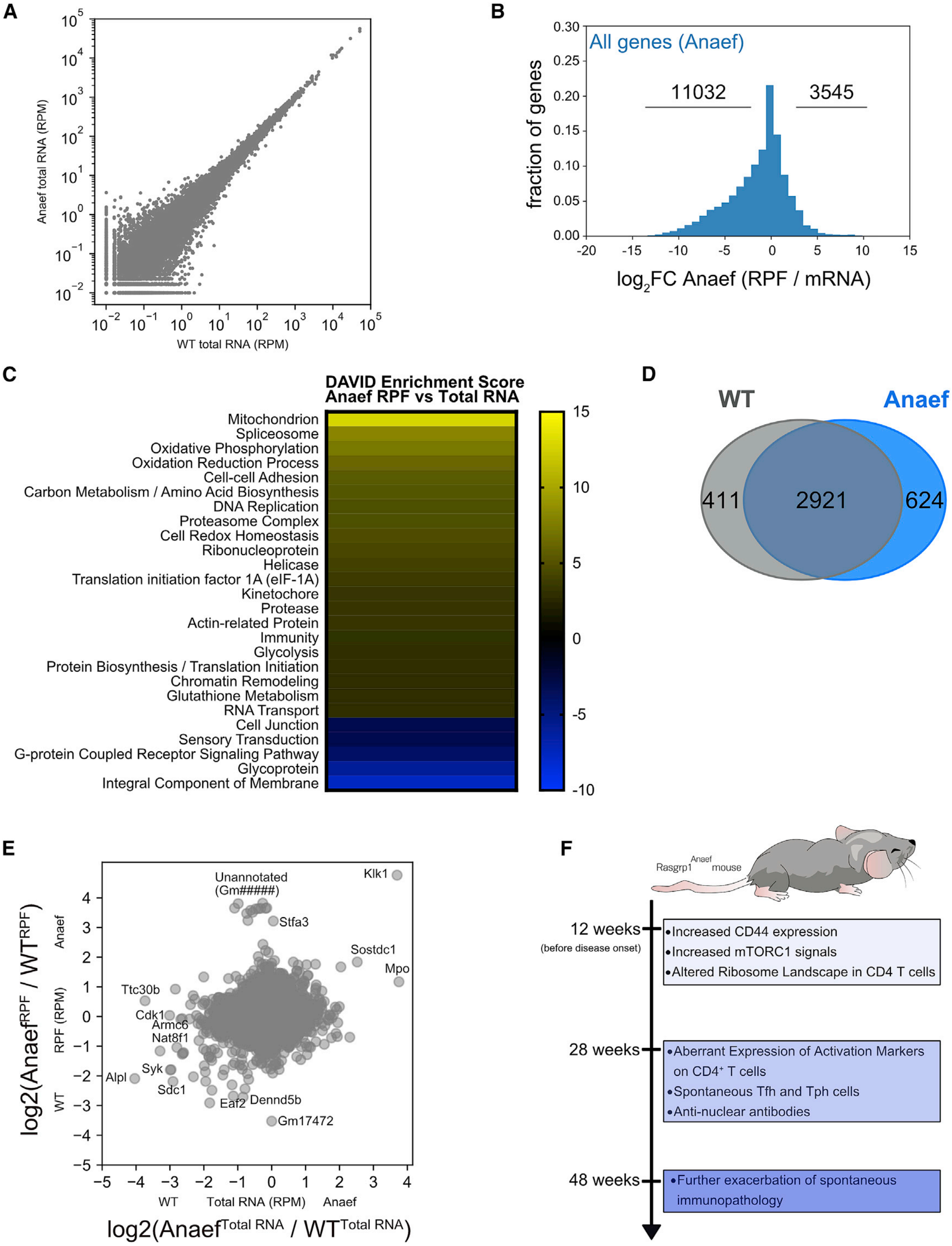

Figure 7. ***$Rasgrp1^{Anaef}$* CD4 T Cells Reveal Subtle Changes in Translational Landscape before Onset of Autoimmunity**

(A) Scatterplot of WT total RNA reads per million (RPM) versus Anaef total RNA reads per million. RPM were averaged across all four biological replicates, a pseudocount of 0.01 was added to all RPM values, and genes that appear in a B cell activation Gene Ontology (GO) signature but not in a T cell activation GO signature were excluded from the plot. Pearson's correlation coefficient (r) was calculated as 0.997.

(B) Histogram plot of DESeq2-calculated log$_2$FC of ribosome-protected fragment (RPF) reads relative to total RNA. The number of genes with a log$_2$FC > 1 are indicated.

(legend continued on next page)

landscape of naive Anaef CD4$^+$ T cells in young animals, prior to the onset of immunopathology (Figure 7F).

DISCUSSION

Over the past decade a hypothesis formed that tonic signals generate low-level phosphorylation to reduce the threshold for T cell activation, priming T cells to respond to infection (Bhandoola et al., 2002; Myers et al., 2017b; Stefanová et al., 2002). However, exclusively reducing the threshold for activation could come at the price of spontaneous autoreactivity. In a previous study, we demonstrated that tonic TCR-LAT signals function as an intrinsic brake. Tonic LAT signals connecting to the epigenetic regulator HDAC7 maintain expression of a set of genes that are negative regulators of T cell proliferation and differentiation (Myers et al., 2017a). In the present study, we establish how tonic Rasgrp1-mTORC1 signals prime the basal state of resting CD4$^+$ T cells by shaping a basal translational landscape. Through genome-wide ribosome profiling, we show that resting primary CD4$^+$ T cells are not at a translational "ground-zero" state during homeostasis but instead have specific translational programs rich in mTOR targets. Our study provides a molecular mechanism for how tonic signals prime the basal state of resting T cells and helps understand published work describing that T cells with the highest tonic signaling and CD5 expression are the best T cell responders during bacterial and viral infections (Fulton et al., 2015; Mandl et al., 2013).

mTOR is known to play a role when the TCR recognizes foreign peptide, leading to T cell activation and differentiation. The cell-biological changes that promote full T cell activation include transcription of mRNAs such as the mTOR target and transcription factor c-Myc (Macintyre et al., 2014; Preston et al., 2015; Verbist et al., 2016; Yang et al., 2013), translation (Chi, 2012; Laplante and Sabatini, 2012), and metabolic reprogramming (MacIver et al., 2013; Pearce et al., 2013). mTOR also relies on input from nutrients such as glucose and amino acids, and this additional input is essential for optimal T cell activation (Macintyre et al., 2014; Sinclair et al., 2013; Zoncu et al., 2011). Here we discovered that the mTORC1 pathway is selectively robust in the basal state in CD4$^+$ T cells *in vivo*. DAVID analysis of pathways points to increased glutathione metabolism at baseline in Anaef T cells, which is an attractive candidate mechanism for how Anaef naive T cells spontaneously take on autoreactive features and cell fates such as Tfh and Tph. In this list of translated target genes unique for Anaef T cells, we noted seven members of the solute carrier family, which are involved in nutrient transport (Table S1). The seven genes have largely been unstudied in T cells, and future work is required to mechanistically link them to immune function in both WT mice and the Anaef model.

T cells with this highest tonic mTORC1 signals polarized more efficiently to Th2 effector cells. Type 2 cell-mediated immunity is associated with protection against helminth parasites. However, because most vertebrates are constantly colonized by helminths (Dobson et al., 2008), type 2 cell immunity may have other functions. Recently, it has become clear that type 2 immunity has important roles in tissue homeostasis (Harris and Loke, 2017). Neonates exhibit exaggerated type 2 immune responses, which aid in the adaptation to the new environment after birth (Torow et al., 2017). This Th2 bias is then likely counterbalanced by subsequent microbial colonization in early childhood (Gollwitzer et al., 2014; Herbst et al., 2011) and reset once again upon helminth infection (Dobson et al., 2008). An interesting concept for future research would be to determine how tonic mTORC1 signals connect to dynamic tissue homeostasis.

Our results here also demonstrate that aberrantly increased tonic mTORC1 signals result in subtle changes in the translational landscape of resting CD4$^+$ T cells and that over time increased tonic mTORC1 signals lead to penetrant immunopathology. This included the development of Tph and Tfh cells over time. Dysregulation of mTORC1 signaling has been previously implicated in autoimmune diseases. T cells from patients with systemic lupus erythematosus (SLE) exhibit mTORC1 activation (Perl, 2016). Rasgrp1 has been implicated in human autoimmune disease as well, as splice variants have been reported in SLE (Yasuda et al., 2007), and single-nucleotide variants were identified from genome-wide association studies (GWAS) on patients with type 1 diabetes and Graves' disease (Plagnol et al., 2011; Qu et al., 2009). The mTORC1 inhibitor rapamycin has been shown to block T cell activation in SLE patients and has therapeutic efficacy in SLE (Perl, 2016). Inhibition of mTORC1 signaling via rapamycin reduced autoimmune features in the Anaef model (Daley et al., 2013) and has been shown to do the same in several other well-established mouse models of SLE (Perl, 2016). Interestingly, a recent study implicated aberrant T cell metabolism, a process regulated by mTOR, as a driver of disease pathology in a mouse model of SLE. Treating mice with both 2-deoxy-D-glucose to block glucose metabolism and metformin to block mitochondrial metabolism restored T cell metabolism to WT levels and led to reduced autoantibodies and lessened kidney pathology (Yin et al., 2015). We saw increased translation of targets in "mitochondria" and "oxidative phosphorylation" cluster; basal translation of these likely support the metabolic state of resting CD4$^+$ T cells, which use mitochondrial oxidative metabolism in the basal state (Gerriets and Rathmell, 2012; MacIver et al., 2013; Pearce et al., 2013). Whether increased tonic mTORC1 signals in T cells is a common

(C) Heatmap of the pathways enriched in the 3,000 most differentially expressed genes (up and down) in the Anaef RPF compared with Anaef total RNA. Functional annotation clustering was performed, and enrichment scores were calculated using DAVID, with the entire Anaef RPF versus Total RNA DESeq2 dataset used as background.

(D) Venn diagram depicting the number of genes that are different or shared between the 3,332 (Figure 6B) and 3,545 (Figure 7B) genes that were increased 2-fold or more in the RPF relative to total RNA for WT and Anaef datasets, respectively.

(E) Scatterplot of the ratio of RPF RPMs for each genotype plotted these against the ratio of the total RNA RPMs for each genotype. Ratios were plotted on a $\log_2$ scale.

(F) Cartoon depicting the kinetics of emerging immunopathology in Rasgrp1^{Anaef} mice.

feature in different autoimmune diseases is an interesting avenue for future study, and could benefit from mouse models such as the *Rasgrp1^{Anaef}* mouse presented here.

STAR★METHODS

Detailed methods are provided in the online version of this paper and include the following:

- KEY RESOURCES TABLE
- CONTACT FOR REAGENT AND RESOURCE SHARING
- EXPERIMENTAL MODEL AND SUBJECT DETAILS
  - ○ Mice
  - ○ Murine Primary Cell Culture
  - ○ DT40 Cell Culture
- METHOD DETAILS
  - ○ HEp-2 ANA Assays
  - ○ Enzyme-Linked Immunosorbent Assay (ELISA)
  - ○ Flow Cytometry
- DATA ANALYSIS
  - ○ DT40 Transfections
  - ○ Inhibitors
  - ○ Immunoblotting
  - ○ qPCR
  - ○ Total RNA Sequencing and Ribosome Profiling
- QUANTIFICATION AND STATISTICAL ANALYSIS
- DATA AND SOFTWARE AVAILABILITY

SUPPLEMENTAL INFORMATION

Supplemental Information can be found online at https://doi.org/10.1016/j.celrep.2019.04.037.

ACKNOWLEDGMENTS

We thank all members of the Roose lab for helpful discussions and Drs. Richard Locksley, Stephen Floor, and Roberto Zoncu for critical reading of the manuscript. We thank the University of California, San Francisco (UCSF), Parnassus Flow Cytometry Core for assistance with cell sorting (NIH grant P30 DK063720); the UCSF Functional Genomics Core (David Erle, Andrea Barczak, Walter Eckalbar, and Matthew Aber) for RNA-seq library preparation; the UCSF Center for Advanced Technology for sequencing; Max Horlbeck for assistance with bioinformatics; and Elizabeth Costa, Dan Santos, Kristen Lynch, and Steve Rosen for helpful discussions on ribosome profiling, splicing, and adhesion. We thank Zoltan Laszik for kidney evaluations, Peter Werba for bioinformatics infrastructure, and Anna Hupalowska for illustrations. These studies were supported by grants from the NSF-GRFP (1650113 to D.R.M.), the Marie Curie IOF (PIOF-GA-2012-328666 to Y.V.), and the NIH-NIAID (R01-AI104789 and P01-AI091580 to J.P.R.).

AUTHOR CONTRIBUTIONS

E.N. and Y.V. performed experiments and analyzed data. D.R.M. performed experiments, analyzed data, and together with J.P.R. conceived the study and wrote the manuscript.

DECLARATION OF INTERESTS

J.P.R. is a co-founder and scientific advisor of Seal Biosciences, Inc., and a member of the scientific advisory committee for the Mark Foundation for Cancer Research.

Received: May 20, 2018
Revised: January 25, 2019
Accepted: April 5, 2019
Published: May 7, 2019

REFERENCES

Ansel, K.M., Djuretic, I., Tanasa, B., and Rao, A. (2006). Regulation of Th2 differentiation and Il4 locus accessibility. Annu. Rev. Immunol. *24*, 607–656.

Araki, K., Morita, M., Bederman, A.G., Konieczny, B.T., Kissick, H.T., Sonenberg, N., and Ahmed, R. (2017). Translation is actively regulated during the differentiation of CD8$^+$ effector T cells. Nat. Immunol. *18*, 1046–1057.

Azzam, H.S., Grinberg, A., Lui, K., Shen, H., Shores, E.W., and Love, P.E. (1998). CD5 expression is developmentally regulated by T cell receptor (TCR) signals and TCR avidity. J. Exp. Med. *188*, 2301–2311.

Baaten, B.J., Cooper, A.M., Swain, S.L., and Bradley, L.M. (2013). Location, location, location: the impact of migratory heterogeneity on T cell function. Front. Immunol. *4*, 311.

Bhandoola, A., Tai, X., Eckhaus, M., Auchincloss, H., Mason, K., Rubin, S.A., Carbone, K.M., Grossman, Z., Rosenberg, A.S., and Singer, A. (2002). Peripheral expression of self-MHC-II influences the reactivity and self-tolerance of mature CD4(+) T cells: evidence from a lymphopenic T cell model. Immunity *17*, 425–436.

Bjur, E., Larsson, O., Yurchenko, E., Zheng, L., Gandin, V., Topisirovic, I., Li, S., Wagner, C.R., Sonenberg, N., and Piccirillo, C.A. (2013). Distinct translational control in CD4+ T cell subsets. PLoS Genet. *9*, e1003494.

Brar, G.A., and Weissman, J.S. (2015). Ribosome profiling reveals the what, when, where and how of protein synthesis. Nat. Rev. *16*, 651–664.

Chi, H. (2012). Regulation and function of mTOR signalling in T cell fate decisions. Nat. Rev. Immunol. *12*, 325–338.

Cook, K.D., and Miller, J. (2010). TCR-dependent translational control of GATA-3 enhances Th2 differentiation. J. Immunol. *185*, 3209–3216.

Daley, S.R., Coakley, K.M., Hu, D.Y., Randall, K.L., Jenne, C.N., Limnander, A., Myers, D.R., Polakos, N.K., Enders, A., Roots, C., et al. (2013). Rasgrp1 mutation increases naive T-cell CD44 expression and drives mTOR-dependent accumulation of Helios$^+$ T cells and autoantibodies. eLife *2*, e01020.

Das, J., Ho, M., Zikherman, J., Govern, C., Yang, M., Weiss, A., Chakraborty, A.K., and Roose, J.P. (2009). Digital signaling and hysteresis characterize ras activation in lymphoid cells. Cell *136*, 337–351.

Delgoffe, G.M., Kole, T.P., Zheng, Y., Zarek, P.E., Matthews, K.L., Xiao, B., Worley, P.F., Kozma, S.C., and Powell, J.D. (2009). The mTOR kinase differentially regulates effector and regulatory T cell lineage commitment. Immunity *30*, 832–844.

Delgoffe, G.M., Pollizzi, K.N., Waickman, A.T., Heikamp, E., Meyers, D.J., Horton, M.R., Xiao, B., Worley, P.F., and Powell, J.D. (2011). The kinase mTOR regulates the differentiation of helper T cells through the selective activation of signaling by mTORC1 and mTORC2. Nat. Immunol. *12*, 295–303.

Dobson, A., Lafferty, K.D., Kuris, A.M., Hechinger, R.F., and Jetz, W. (2008). Colloquium paper: homage to Linnaeus: how many parasites? How many hosts? Proc. Natl. Acad. Sci. U S A *105* (*Suppl 1*), 11482–11489.

Dunn, J.G., and Weissman, J.S. (2016). Plastid: nucleotide-resolution analysis of next-generation sequencing and genomics data. BMC Genomics *17*, 958.

Fischer, A.M., Katayama, C.D., Pagès, G., Pouysségur, J., and Hedrick, S.M. (2005). The role of erk1 and erk2 in multiple stages of T cell development. Immunity *23*, 431–443.

Fu, X.D., and Ares, M., Jr. (2014). Context-dependent control of alternative splicing by RNA-binding proteins. Nat. Rev. *15*, 689–701.

Fulton, R.B., Hamilton, S.E., Xing, Y., Best, J.A., Goldrath, A.W., Hogquist, K.A., and Jameson, S.C. (2015). The TCR's sensitivity to self peptide-MHC dictates the ability of naive CD8(+) T cells to respond to foreign antigens. Nat. Immunol. *16*, 107–117.

Gentilella, A., and Thomas, G. (2012). Cancer biology: the director's cut. Nature *485*, 50–51.

Gerriets, V.A., and Rathmell, J.C. (2012). Metabolic pathways in T cell fate and function. Trends Immunol. *33*, 168–173.

Gigoux, M., Lovato, A., Leconte, J., Leung, J., Sonenberg, N., and Suh, W.K. (2014). Inducible costimulator facilitates T-dependent B cell activation by augmenting IL-4 translation. Mol. Immunol. *59*, 46–54.

Gollwitzer, E.S., Saglani, S., Trompette, A., Yadava, K., Sherburn, R., McCoy, K.D., Nicod, L.P., Lloyd, C.M., and Marsland, B.J. (2014). Lung microbiota promotes tolerance to allergens in neonates via PD-L1. Nat. Med. *20*, 642–647.

Gorentla, B.K., Wan, C.K., and Zhong, X.P. (2011). Negative regulation of mTOR activation by diacylglycerol kinases. Blood *117*, 4022–4031.

Guttman, M., Russell, P., Ingolia, N.T., Weissman, J.S., and Lander, E.S. (2013). Ribosome profiling provides evidence that large noncoding RNAs do not encode proteins. Cell *154*, 240–251.

Harris, N.L., and Loke, P. (2017). Recent advances in type-2-cell-mediated immunity: insights from Helminth infection. Immunity *47*, 1024–1036.

Heikamp, E.B., Patel, C.H., Collins, S., Waickman, A., Oh, M.H., Sun, I.H., Illei, P., Sharma, A., Naray-Fejes-Toth, A., Fejes-Toth, G., et al. (2014). The AGC kinase SGK1 regulates TH1 and TH2 differentiation downstream of the mTORC2 complex. Nat. Immunol. *15*, 457–464.

Herbst, T., Sichelstiel, A., Schär, C., Yadava, K., Bürki, K., Cahenzli, J., McCoy, K., Marsland, B.J., and Harris, N.L. (2011). Dysregulation of allergic airway inflammation in the absence of microbial colonization. Am. J. Respir. Crit. Care Med. *184*, 198–205.

Hogquist, K.A., Starr, T.K., and Jameson, S.C. (2003). Receptor sensitivity: when T cells lose their sense of self. Curr. Biol. *13*, R239–R241.

Hogquist, K.A., Baldwin, T.A., and Jameson, S.C. (2005). Central tolerance: learning self-control in the thymus. Nat. Rev. Immunol. *5*, 772–782.

Hsieh, A.C., Liu, Y., Edlind, M.P., Ingolia, N.T., Janes, M.R., Sher, A., Shi, E.Y., Stumpf, C.R., Christensen, C., Bonham, M.J., et al. (2012). The translational landscape of mTOR signalling steers cancer initiation and metastasis. Nature *485*, 55–61.

Huang, W., Sherman, B.T., and Lempicki, R.A. (2009). Systematic and integrative analysis of large gene lists using DAVID bioinformatics resources. Nat. Protoc. *4*, 44–57.

Ingolia, N.T., Brar, G.A., Rouskin, S., McGeachy, A.M., and Weissman, J.S. (2013). Genome-wide annotation and quantitation of translation by ribosome profiling. Curr. Protoc. Mol. Biol. *Chapter 4*, Unit 4.18.

Iwig, J.S., Vercoulen, Y., Das, R., Barros, T., Limnander, A., Che, Y., Pelton, J.G., Wemmer, D.E., Roose, J.P., and Kuriyan, J. (2013). Structural analysis of autoinhibition in the Ras-specific exchange factor RasGRP1. eLife *2*, e00813.

Krutzik, P.O., and Nolan, G.P. (2006). Fluorescent cell barcoding in flow cytometry allows high-throughput drug screening and signaling profiling. Nat. Methods *3*, 361–368.

Ksionda, O., Limnander, A., and Roose, J.P. (2013). RasGRP Ras guanine nucleotide exchange factors in cancer. Front. Biol. (Beijing) *8*, 508–532.

Ksionda, O., Mues, M., Wandler, A.M., Donker, L., Tenhagen, M., Jun, J., Ducker, G.S., Matlawska-Wasowska, K., Shannon, K., Shokat, K.M., and Roose, J.P. (2018). Comprehensive analysis of T cell leukemia signals reveals heterogeneity in the PI3 kinase-Akt pathway and limitations of PI3 kinase inhibitors as monotherapy. PLoS ONE *13*, e0193849.

Langmead, B., Trapnell, C., Pop, M., and Salzberg, S.L. (2009). Ultrafast and memory-efficient alignment of short DNA sequences to the human genome. Genome Biol. *10*, R25.

Laplante, M., and Sabatini, D.M. (2012). mTOR signaling in growth control and disease. Cell *149*, 274–293.

Li, H., Handsaker, B., Wysoker, A., Fennell, T., Ruan, J., Homer, N., Marth, G., Abecasis, G., and Durbin, R.; 1000 Genome Project Data Processing Subgroup (2009). The Sequence Alignment/Map format and SAMtools. Bioinformatics *25*, 2078–2079.

Liu, X., Nurieva, R.I., and Dong, C. (2013). Transcriptional regulation of follicular T-helper (Tfh) cells. Immunol. Rev. *252*, 139–145.

Love, M.I., Huber, W., and Anders, S. (2014). Moderated estimation of fold change and dispersion for RNA-seq data with DESeq2. Genome Biol. *15*, 550.

Macintyre, A.N., Gerriets, V.A., Nichols, A.G., Michalek, R.D., Rudolph, M.C., Deoliveira, D., Anderson, S.M., Abel, E.D., Chen, B.J., Hale, L.P., and Rathmell, J.C. (2014). The glucose transporter Glut1 is selectively essential for CD4 T cell activation and effector function. Cell Metab. *20*, 61–72.

MacIver, N.J., Michalek, R.D., and Rathmell, J.C. (2013). Metabolic regulation of T lymphocytes. Annu. Rev. Immunol. *31*, 259–283.

Mak, T.W., Grusdat, M., Duncan, G.S., Dostert, C., Nonnenmacher, Y., Cox, M., Binsfeld, C., Hao, Z., Brüstle, A., Itsumi, M., et al. (2017). Glutathione primes T cell metabolism for inflammation. Immunity *46*, 675–689.

Mandl, J.N., Monteiro, J.P., Vrisekoop, N., and Germain, R.N. (2013). T cell-positive selection uses self-ligand binding strength to optimize repertoire recognition of foreign antigens. Immunity *38*, 263–274.

Markegard, E., Trager, E., Yang, C.W., Zhang, W., Weiss, A., and Roose, J.P. (2011). Basal LAT-diacylglycerol-RasGRP1 signals in T cells maintain TCRα gene expression. PLoS ONE *6*, e25540.

Martinez, N.M., and Lynch, K.W. (2013). Control of alternative splicing in immune responses: many regulators, many predictions, much still to learn. Immunol. Rev. *253*, 216–236.

Marzluff, W.F., Wagner, E.J., and Duronio, R.J. (2008). Metabolism and regulation of canonical histone mRNAs: life without a poly(A) tail. Nat. Rev. *9*, 843–854.

Meister, A. (1983). Selective modification of glutathione metabolism. Science *220*, 472–477.

Moran, A.E., Holzapfel, K.L., Xing, Y., Cunningham, N.R., Maltzman, J.S., Punt, J., and Hogquist, K.A. (2011). T cell receptor signal strength in Treg and iNKT cell development demonstrated by a novel fluorescent reporter mouse. J. Exp. Med. *208*, 1279–1289.

Myers, D.R., Lau, T., Markegard, E., Lim, H.W., Kasler, H., Zhu, M., Barczak, A., Huizar, J.P., Zikherman, J., Erle, D.J., et al. (2017a). Tonic LAT-HDAC7 signals sustain Nur77 and Irf4 expression to tune naive CD4 T cells. Cell Rep. *19*, 1558–1571.

Myers, D.R., Zikherman, J., and Roose, J.P. (2017b). Tonic signals: why do lymphocytes bother? Trends Immunol. *38*, 844–857.

O'Shea, J.J., and Paul, W.E. (2010). Mechanisms underlying lineage commitment and plasticity of helper CD4+ T cells. Science *327*, 1098–1102.

Oh-hora, M., Johmura, S., Hashimoto, A., Hikida, M., and Kurosaki, T. (2003). Requirement for Ras guanine nucleotide releasing protein 3 in coupling phospholipase C-gamma2 to Ras in B cell receptor signaling. J. Exp. Med. *198*, 1841–1851.

Oki-Idouchi, C.E., and Lorenzo, P.S. (2007). Transgenic overexpression of RasGRP1 in mouse epidermis results in spontaneous tumors of the skin. Cancer Res. *67*, 276–280.

Ouyang, W., Löhning, M., Gao, Z., Assenmacher, M., Ranganath, S., Radbruch, A., and Murphy, K.M. (2000). Stat6-independent GATA-3 autoactivation directs IL-4-independent Th2 development and commitment. Immunity *12*, 27–37.

Paul, W.E. (2010). What determines Th2 differentiation, in vitro and in vivo? Immunol. Cell Biol. *88*, 236–239.

Pearce, E.L., Poffenberger, M.C., Chang, C.H., and Jones, R.G. (2013). Fueling immunity: insights into metabolism and lymphocyte function. Science *342*, 1242454.

Perl, A. (2016). Activation of mTOR (mechanistic target of rapamycin) in rheumatic diseases. Nat. Rev. Rheumatol. *12*, 169–182.

Persaud, S.P., Parker, C.R., Lo, W.L., Weber, K.S., and Allen, P.M. (2014). Intrinsic CD4+ T cell sensitivity and response to a pathogen are set and sustained by avidity for thymic and peripheral complexes of self peptide and MHC. Nat. Immunol. *15*, 266–274.

Piccirillo, C.A., Bjur, E., Topisirovic, I., Sonenberg, N., and Larsson, O. (2014). Translational control of immune responses: from transcripts to translatomes. Nat. Immunol. *15*, 503–511.

Plagnol, V., Howson, J.M., Smyth, D.J., Walker, N., Hafler, J.P., Wallace, C., Stevens, H., Jackson, L., Simmonds, M.J., Bingley, P.J., et al.; Type 1 Diabetes Genetics Consortium (2011). Genome-wide association analysis of autoantibody positivity in type 1 diabetes cases. PLoS Genet. *7*, e1002216.

Powell, J.D., and Delgoffe, G.M. (2010). The mammalian target of rapamycin: linking T cell differentiation, function, and metabolism. Immunity *33*, 301–311.

Powell, J.D., Pollizzi, K.N., Heikamp, E.B., and Horton, M.R. (2012). Regulation of immune responses by mTOR. Annu. Rev. Immunol. *30*, 39–68.

Preston, G.C., Sinclair, L.V., Kaskar, A., Hukelmann, J.L., Navarro, M.N., Ferrero, I., MacDonald, H.R., Cowling, V.H., and Cantrell, D.A. (2015). Single cell tuning of Myc expression by antigen receptor signal strength and interleukin-2 in T lymphocytes. EMBO J. *34*, 2008–2024.

Qu, H.Q., Grant, S.F., Bradfield, J.P., Kim, C., Frackelton, E., Hakonarson, H., and Polychronakos, C. (2009). Association of RASGRP1 with type 1 diabetes is revealed by combined follow-up of two genome-wide studies. J. Med. Genet. *46*, 553–554.

Rao, D.A., Gurish, M.F., Marshall, J.L., Slowikowski, K., Fonseka, C.Y., Liu, Y., Donlin, L.T., Henderson, L.A., Wei, K., Mizoguchi, F., et al. (2017). Pathologically expanded peripheral T helper cell subset drives B cells in rheumatoid arthritis. Nature *542*, 110–114.

Roux, P.P., Shahbazian, D., Vu, H., Holz, M.K., Cohen, M.S., Taunton, J., Sonenberg, N., and Blenis, J. (2007). RAS/ERK signaling promotes site-specific ribosomal protein S6 phosphorylation via RSK and stimulates cap-dependent translation. J. Biol. Chem. *282*, 14056–14064.

Saxton, R.A., and Sabatini, D.M. (2017). mTOR signaling in growth, metabolism, and disease. Cell *168*, 960–976.

Scheu, S., Stetson, D.B., Reinhardt, R.L., Leber, J.H., Mohrs, M., and Locksley, R.M. (2006). Activation of the integrated stress response during T helper cell differentiation. Nat. Immunol. *7*, 644–651.

Sinclair, L.V., Rolf, J., Emslie, E., Shi, Y.B., Taylor, P.M., and Cantrell, D.A. (2013). Control of amino-acid transport by antigen receptors coordinates the metabolic reprogramming essential for T cell differentiation. Nat. Immunol. *14*, 500–508.

So, L., Lee, J., Palafox, M., Mallya, S., Woxland, C.G., Arguello, M., Truitt, M.L., Sonenberg, N., Ruggero, D., and Fruman, D.A. (2016). The 4E-BP-eIF4E axis promotes rapamycin-sensitive growth and proliferation in lymphocytes. Sci. Signal. *9*, ra57.

Stefanová, I., Dorfman, J.R., and Germain, R.N. (2002). Self-recognition promotes the foreign antigen sensitivity of naive T lymphocytes. Nature *420*, 429–434.

Stern-Ginossar, N., Weisburd, B., Michalski, A., Le, V.T., Hein, M.Y., Huang, S.X., Ma, M., Shen, B., Qian, S.B., Hengel, H., et al. (2012). Decoding human cytomegalovirus. Science *338*, 1088–1093.

Tan, T.C.J., Knight, J., Sbarrato, T., Dudek, K., Willis, A.E., and Zamoyska, R. (2017). Suboptimal T-cell receptor signaling compromises protein translation, ribosome biogenesis, and proliferation of mouse CD8 T cells. Proc. Natl. Acad. Sci. U S A *114*, E6117–E6126.

Thoreen, C.C., Chantranupong, L., Keys, H.R., Wang, T., Gray, N.S., and Sabatini, D.M. (2012). A unifying model for mTORC1-mediated regulation of mRNA translation. Nature *485*, 109–113.

Torow, N., Marsland, B.J., Hornef, M.W., and Gollwitzer, E.S. (2017). Neonatal mucosal immunology. Mucosal Immunol. *10*, 5–17.

Trapnell, C., Pachter, L., and Salzberg, S.L. (2009). TopHat: discovering splice junctions with RNA-Seq. Bioinformatics *25*, 1105–1111.

van den Brink, M.R., Kapeller, R., Pratt, J.C., Chang, J.H., and Burakoff, S.J. (1999). The extracellular signal-regulated kinase pathway is required for activation-induced cell death of T cells. J. Biol. Chem. *274*, 11178–11185.

van Oers, N.S., Tao, W., Watts, J.D., Johnson, P., Aebersold, R., and Teh, H.S. (1993). Constitutive tyrosine phosphorylation of the T-cell receptor (TCR) zeta subunit: regulation of TCR-associated protein tyrosine kinase activity by TCR zeta. Mol. Cell. Biol. *13*, 5771–5780.

van Oers, N.S., Killeen, N., and Weiss, A. (1994). ZAP-70 is constitutively associated with tyrosine-phosphorylated TCR zeta in murine thymocytes and lymph node T cells. Immunity *1*, 675–685.

Verbist, K.C., Guy, C.S., Milasta, S., Liedmann, S., Kamiński, M.M., Wang, R., and Green, D.R. (2016). Metabolic maintenance of cell asymmetry following division in activated T lymphocytes. Nature *532*, 389–393.

Waickman, A.T., and Powell, J.D. (2012). mTOR, metabolism, and the regulation of T-cell differentiation and function. Immunol. Rev. *249*, 43–58.

Wikenheiser, D.J., and Stumhofer, J.S. (2016). ICOS co-stimulation: friend or foe? Front. Immunol. *7*, 304.

Yang, K., Shrestha, S., Zeng, H., Karmaus, P.W., Neale, G., Vogel, P., Guertin, D.A., Lamb, R.F., and Chi, H. (2013). T cell exit from quiescence and differentiation into Th2 cells depend on Raptor-mTORC1-mediated metabolic reprogramming. Immunity *39*, 1043–1056.

Yang, J., Lin, X., Pan, Y., Wang, J., Chen, P., Huang, H., Xue, H.H., Gao, J., and Zhong, X.P. (2016). Critical roles of mTOR Complex 1 and 2 for T follicular helper cell differentiation and germinal center responses. eLife *5*, e17936.

Yasuda, S., Stevens, R.L., Terada, T., Takeda, M., Hashimoto, T., Fukae, J., Horita, T., Kataoka, H., Atsumi, T., and Koike, T. (2007). Defective expression of Ras guanyl nucleotide-releasing protein 1 in a subset of patients with systemic lupus erythematosus. J. Immunol. *179*, 4890–4900.

Yin, Y., Choi, S.C., Xu, Z., Perry, D.J., Seay, H., Croker, B.P., Sobel, E.S., Brusko, T.M., and Morel, L. (2015). Normalization of CD4+ T cell metabolism reverses lupus. Sci. Transl. Med. *7*, 274ra18.

Zeng, H., Yang, K., Cloer, C., Neale, G., Vogel, P., and Chi, H. (2013). mTORC1 couples immune signals and metabolic programming to establish T(reg)-cell function. Nature *499*, 485–490.

Zeng, H., Cohen, S., Guy, C., Shrestha, S., Neale, G., Brown, S.A., Cloer, C., Kishton, R.J., Gao, X., Youngblood, B., et al. (2016). mTORC1 and mTORC2 kinase signaling and glucose metabolism drive follicular helper T cell differentiation. Immunity *45*, 540–554.

Zhang, S., Readinger, J.A., DuBois, W., Janka-Junttila, M., Robinson, R., Pruitt, M., Bliskovsky, V., Wu, J.Z., Sakakibara, K., Patel, J., et al. (2011). Constitutive reductions in mTOR alter cell size, immune cell development, and antibody production. Blood *117*, 1228–1238.

Zikherman, J., Jenne, C., Watson, S., Doan, K., Raschke, W., Goodnow, C.C., and Weiss, A. (2010). CD45-Csk phosphatase-kinase titration uncouples basal and inducible T cell receptor signaling during thymic development. Immunity *32*, 342–354.

Zikherman, J., Parameswaran, R., and Weiss, A. (2012). Endogenous antigen tunes the responsiveness of naive B cells but not T cells. Nature *489*, 160–164.

Zoncu, R., Efeyan, A., and Sabatini, D.M. (2011). mTOR: from growth signal integration to cancer, diabetes and ageing. Nat. Rev. *12*, 21–35.

STAR★METHODS

KEY RESOURCES TABLE

REAGENT or RESOURCE	SOURCE	IDENTIFIER
Antibodies		
ICOS (fluorophore-conjugated, anti-mouse)	Biolegend	Clone 7E.17G9
CD279 (PD1) (fluorophore-conjugated, anti-mouse)	Biolegend	Clone RMP1-30; AB_572016
CXCR5 (fluorophore-conjugated, anti-mouse)	Biolegend	Clone L138D7; AB_2561969
CD4 (fluorophore-conjugated, anti-mouse)	Tonbo Biosciences	Clone RM4-5
CD8 (fluorophore-conjugated, anti-mouse)	BD Biosciences	Clone 53-6.7
TCRb (fluorophore-conjugated, anti-mouse)	Biolegend	Clone H57-597
CD44 (fluorophore-conjugated, anti-mouse)	Tonbo Biosciences	Clone IM7
CD62L (fluorophore-conjugated, anti-mouse)	BD Biosciences	Clone Mel-14
CD25 (fluorophore-conjugated, anti-mouse)	Tonbo Biosciences	Clone PC61
CD69 (fluorophore-conjugated, anti-mouse)	BD Biosciences	Clone HI.2F3
CD5 (fluorophore-conjugated, anti-mouse)	53-7.3	Clone 53-7.3
CD11b (fluorophore-conjugated, anti-mouse)	BD Biosciences	Clone M1/70
CD11c (fluorophore-conjugated, anti-mouse)	BD Biosciences	Clone HL3
CD19 (fluorophore-conjugated, anti-mouse)	BD Biosciences	Clone 1D3
B220 (fluorophore-conjugated, anti-mouse)	BD Biosciences	Clone RA3-6B2
Ter119 (fluorophore-conjugated, anti-mouse)	BD Biosciences	Clone TER-119
CD49b (fluorophore-conjugated, anti-mouse)	BD Biosciences	Clone DX5
Gr1 (fluorophore-conjugated, anti-mouse)	Biolegend	Clone RB6-8C5
IFNg (fluorophore-conjugated, anti-mouse)	eBioscience	Clone XMG1.2
IL-4 (fluorophore-conjugated, anti-mouse)	BD Biosciences	Clone 11B11
IL-17A (fluorophore-conjugated, anti-mouse)	eBioscience	Clone eBio17B7
FoxP3 (fluorophore-conjugated, anti-mouse)	eBioscience	Clone FJK-16 s
Gata3 (fluorophore-conjugated, anti-mouse)	eBioscience	Clone TWAJ
Bcl6 (fluorophore-conjugated, anti-mouse)	BD Biosciences	Clone K112-91
P-S6 S235/236 (unconjugated, anti-mouse)	Cell Signaling Technologies	Cat# 2211; AB_331679
P-S6 S240/244 (unconjugated, anti-mouse)	Cell Signaling Technologies	Cat#2215; AB_331682
P-44/42 MAPK (P-Erk) (unconjugated, anti-mouse)	Cell Signaling Technologies	Cat#4377; AB_331775
P-Akt S473 (unconjugated, anti-mouse)	Cell Signaling Technologies	Cat#4058; AB_331168
Donkey anti-Rabbit IgG secondary (PE conjugated, for flow cytometry)	Jackson Immunoresearch	Cat# 711-116-152; AB_2340599

(*Continued on next page*)

Continued

REAGENT or RESOURCE	SOURCE	IDENTIFIER
Donkey anti-Rabbit IgG secondary (APC conjugated, for flow cytometry)	Jackson Immunoresearch	Cat# 711-136-152; AB_2340601
Gata3 (immunoblotting; mouse monoclonal)	Santa Cruz Biotechnologies	Cat# SC-268; AB_2108591
TBP (immunoblotting; rabbit polyclonal)	Cell Signaling Technologies	Cat# 8515; AB_10949159
anti-mouse CD3 (T cell stimulations; unconjugated)	Tonbo Biosciences	Clone 2C11
anti-mouse CD28 (T cell stimulations; unconjugated)	Tonbo Biosciences	Clone 37.51
Donkey anti-Mouse IgG (H+L) FITC secondary (ELISA)	Jackson Immunoresearch	Cat# 715-095-150; AB_2340792
Goat anti-Mouse Ig	Southern Biotech	Cat# SB1010-01
anti-IgA-HRP	Southern Biotech	Cat# SB1040-05
anti-IgG3-HRP	Southern Biotech	Cat# SB1100-05
anti-IgG1-HRP	Southern Biotech	Cat# SB1070-05
anti-IgM-HRP	Southern Biotech	Cat# SB1020-05
anti-IgG2b-HRP	Southern Biotech	Cat# SB1090-05
anti-IgG-HRP	Southern Biotech	Cat# SB1020-05
Chemicals, Peptides, and Recombinant Proteins		
Recombinant murine IL-12	Peprotech	Cat# 210-12
Recombinant murine IL-4	Peprotech	Cat# AF-214-14
Recombinant human TGFb	R&D Systems	Cat# 240-B-002
Recombinant murine IL-6	Peprotech	Cat# 216-16
Anti-IL-4	UCSF Monoclonal Antibody Core	Clone 11B11
Anti-IFNg	UCSF Monoclonal Antibody Core	Clone XMG1.2
DAPI	Thermo Fisher Scientific	Cat# D1306
TMB Solution	Sigma Aldrich	Cat# T4319
Phorbol-12-myristate-13-acetate (PMA)	EMD Millipore	Cat# 524400
Ionomycin	Sigma Aldrich	Cat# I0634
BD Golgi Stop	BD Biosciences	Cat# 554724
Live/Dead Fixable Viability Dye	Thermo Fisher Scientific	Cat# L34955
Fixation/Permeabilization Solution Kit	BD Biosciences	Cat# 554714
FoxP3 Fixation/Permeabilization Buffer Set	eBioscience	Cat# 00-5523-00
Succinimidyl Esters (for fluorescent cellular barcoding)	Thermo Fisher Scientific / Molecular Probes	Cat# A20000 (AF488), Cat# P10163 (Pacific Blue)
Rapamycin	EMD Millipore	Cat# 553211
BI-D1870	Enzo Life Sciences	Cat# BML-EI407-0001
DNase I	Thermo Fisher Scientific	Cat# 12185010
Super Script IV first-strand synthesis kit	Thermo Fisher Scientific	Cat# 18091050
Cycloheximide	Sigma Aldrich	Cat# C4859
Critical Commercial Assays		
Naive CD4 T cell Isolation Kit (mouse)	Miltenyi Biotec	Cat# 130-104-453
Nova-Lite HEp-2 ANA Kit	INOVA Diagnostics	Cat# 508100.2
PicoPure® RNA Isolation Kit	Thermo Fisher Scientific	Cat# KIT0214
TaqMan Fast Advanced Master Mix	Applied Biosciences	Cat# 4444963
Dynabeads mRNA DIRECT Purification Kit	Thermo Fisher Scientific	Cat# 61011
TruSeq Ribo Profile (Mammalian) kit	Illumina	Cat# RPHMR12126

(*Continued on next page*)

Continued

REAGENT or RESOURCE	SOURCE	IDENTIFIER
Deposited Data		
Mouse reference genome NCBI build 38, GRCm38	Genome Reference Consortium	https://www.ncbi.nlm.nih.gov/assembly/GCF_000001635.20/
RNA Sequencing of WT and Anaef CD4+ T cells	This paper	GEO: GSE114741
Ribosome Profiling of WT and Anaef CD4+ T cells	This paper	GEO: GSE114741
Experimental Models: Cell Lines		
Chicken B cells: WT DT40 Rasgrp1−/−/3 double deficient)	Oh-hora et al., 2003	RRID: CVCL_0249
Chicken B cells: Rasgrp1−/− Rasgrp3−/−	Oh-hora et al., 2003	RRID: CVCL1U39
Experimental Models: Organisms/Strains		
Mouse: Nur77-GFP	Drs. Art Weiss and Julie Zikherman; Zikherman et al., 2012	N/A
Mouse: Rasgrp1$^{\text{Anaef}}$	Daley et al., 2013	RRID: MGI:5564911
Mouse: OT-II TCR Transgenic	UCSF Mouse Inventory	N/A
Oligonucleotides		
qPCR primers/probes for CD44	Life Technologies	Assay ID Mm01277161_m1
qPCR primers/probes for Gata3	Life Technologies	Assay ID Mm00484683_m1
qPCR primers/probes for Ppia	Life Technologies	Assay ID Mm02342430_g1
Recombinant DNA		
pEGFP-N1-Rasgrp1 WT-EGFP	Iwig et al., 2013	N/A
pEGFP-N1-Rasgrp1 R271E-EGFP	Iwig et al., 2013	N/A
pEGFP-N1-Rasgrp1-R519G-EGFP	Iwig et al., 2013	N/A
Software and Algorithms		
TopHat v1.4.1	Trapnell et al., 2009	https://ccb.jhu.edu/software/tophat/index.shtml
Bowtie v0.12.7	Langmead et al., 2009	http://bowtie-bio.sourceforge.net/index.shtml
Samtools v0.1.18	Li et al., 2009	http://samtools.sourceforge.net/
Plastid	Dunn and Weissman, 2016	https://plastid.readthedocs.io/en/latest/
DESeq2	Love et al., 2014	https://bioconductor.org/packages/release/bioc/html/DESeq2.html
DAVID	Huang et al., 2009	https://david.ncifcrf.gov/

CONTACT FOR REAGENT AND RESOURCE SHARING

Further information and requests for resources and reagents should be directed to and will be fulfilled by the Lead Contact, Jeroen Roose (Jeroen.Roose@ucsf.edu).

EXPERIMENTAL MODEL AND SUBJECT DETAILS

Mice

WT C57BL/6 mice and OT-II TCR transgenic mice were bred in house at UCSF. Nur77-GFP mice were obtained from Drs. Arthur Weiss and Julie Zikherman and have been described previously (Zikherman et al., 2012). Rasgrp1$^{\text{Anaef}}$ mice have been described previously (Daley et al., 2013) and were bred at UCSF. Mice used in experiments were between 8 and 12 weeks unless otherwise indicated. For *in vivo* studies with rapamycin treatments, mice were 12 weeks of age. Both male and female mice were used, with approximate weights of 20 g and 27 g, respectively. Littermates of the same genotype were randomly assigned into vehicle and rapamycin treated groups. Animals had not previously had any drug treatments or procedures performed on them. Mice were housed and treated in accordance with the guidelines of the Institutional Animal Care and Use Committee (IACUC) guidelines of the University of California, San Francisco (AN098375-03B).

Murine Primary Cell Culture

Cells were isolated from cervical, brachial, axillary, inguinal, and mesenteric lymph nodes of mice, with both male and female mice being used in experiments. $CD4^+$ T cells were isolated by MACS negative isolation (Miltenyi) or by fluorescent activated cell sorting (FACS; staining for CD4, CD25, CD44, and CD5) in the UCSF Flow Cytometry Core. Cells were counted and plated on 96 well plates that had been pre-coated with 2ug/ml α-CD3 and 2ug/ml α-CD28 unless otherwise indicated. T cells were cultured in RPMI (Hyclone) supplemented with 10% fetal calf serum, 1% sodium pyruvate, 1% nonessential amino acids, 1% HEPES, 1% pen-strep-glutamine, and 0.1% beta mercaptoethanol, at 37°C. For differentiation assays, cells were cultured in media supplemented with cytokines and blocking antibodies as follows: Th1 conditions 10ng/ml rIL-12 (Peprotech) and 10ug/ml anti-IL-4 clone 11B11 (UCSF mAb core); Th2 conditions (10ng/ml rIL-4 (Peprotech) and 10ug/ml anti-IFNγ clone XMG1.2 (UCSF mAb core); Th17 conditions 1ng/ml TGFb (R&D Systems), 40ng/ml rIL-6 (Peprotech), 10ug/ml a-IFNγ clone XMG1.2; iTreg conditions 2ug/ml TGFb. Th1 and Th2 cells were cultured for 3 days on plate-bound stimulation, then rested in complete media without stimulation for two days prior to intracellular cytokine staining. Th17 and iTreg cells were cultured for 4 days on plate-bound stimulation prior to intracellular cytokine or transcription factor staining.

DT40 Cell Culture

Rasgrp1-WT and *Rasgrp1/3*-deficient DT40 chicken B cells were maintained in RPMI supplemented with 10%FBS, 1% chicken serum, 1% pen-strep-glutamine, and 2.5% HEPES at 37°C. Cells were cultured between 0.2 and 1 million / mL. DT40 cells are female (ZW). These cell lines were originally described in Oh-hora et al. (2003). The lines used in this study were authenticated are tested negative for Mycoplasma.

METHOD DETAILS

HEp-2 ANA Assays

HEp-2 assays were performed utilizing the Nova-Lite kit from INOVA diagnostics. Serum was applied to slides, stained with IgG-FITC (Jackson Labs) and DAPI (500ng/ml, Thermo Fisher Scientific). Slides were imaged on a Keyensce BZ-X710 microscope. Sera were scored as ANA negative or ANA positive based on a no serum negative control or a CD45 Wedge B6-129 F1 positive control serum (a gift from Michelle Hermiston's lab) present on each slide.

Enzyme-Linked Immunosorbent Assay (ELISA)

Plates were pre-coated with Goat anti-Mouse Ig (Southern Biotech), blocked with PBS-BB (PBS + 0.05% Tween 20 + 1% BSA) and serum was applied. HRP conjugated secondary antibodies anti-IgA-HRP, anti-IgG3-HRP, anti-IgG1-HRP, anti-IgM-HRP, anti-IgG2b-HRP, and anti-IgG-HRP (all from Southern Biotech) were applied and subsequently exposed with a slow kinetic TMB solution (Sigma). The reaction was terminated with 1N HCL and absorbance was measured at 450 nm on a SpectraMax 340 PC plate reader and analyzed using SoftMax Pro 4.8 Software.

Flow Cytometry

Antibodies

Fluorophore-conjugated ICOS, PD1, CXCR5, CD4, CD8, TCRβ, CD44, CD62L, CD25, CD69, CD5, CD11b, CD11c, CD19, B220, Ter119, DX5, Gr1, IFNγ, IL-4, IL-17A, FoxP3, Gata3, and Bcl6 were purchased from eBioscience, BD Biosciences, BioLegend, and Tonbo Biosciences. Primary antibodies for phospho-flow cytometry were purchased from Cell Signaling Technologies: P-S6 S235/236 (2211), P-S6 S240/244 (2215), P-ERK (4377), and P-Akt (4058). Secondary antibody for phospho-flow cytometry was R-Phycoerythrin AffiniPure $F(ab')_2$ Fragment Donkey Anti-Rabbit IgG (Jackson Immunoresearch).

Tfh cell analysis

Peyer's Patches were isolated from mice and stained with antibodies to B220, CD4, PD-1, CXCR5 (Biolegend, clone L138D7) for 1 hour at room temperature prior to analysis by flow cytometry.

Intracellular cytokine staining

Cells were harvested, restimulated in complete media supplemented with 5ng/ml PMA (EMD Millipore) and 500ng/ml ionomycin (Sigma Aldrich) for 1 hour at 37°C, and then in the same media supplemented with monensin (BD Golgi Stop) for an additional 3 hours. Restimulated cells were washed, stained with Live/Dead Fixable Violet dye (Thermo Fisher Scientific), stained for relevant surface markers where applicable, and then fixed in BD Cytofix/Cytoperm buffer. Membranes were permeabilized with BD Perm/Wash buffer and stained with anti-cytokine antibodies (eBioscience IFNγ clone XMG1.2; BD IL-4 clone 11B11; eBioscience IL-17A clone eBio17B7) prior to analysis by flow cytometry.

Phospho-flow cytometry and fluorescent cellular barcoding

Cells were harvested at indicated time points, washed, and either rested in full culture media (but lacking FCS) for the indicated time points or directly fixed in 2% PFA. Membranes were permeabilized with ice-cold 90% methanol at −20°C, and subsequently cells were barcoded with Alexa Fluor 488 (final dye concentrations of 15, 5, 1.3, 0.3, 0.075 ug/ml) and Pacific Blue (final dye concentrations of 40, 6.5, 0.6, 0.075 ug/ml) succinimidyl esters (Thermo Fisher / Molecular Probes). Barcoded cells were pooled and the bulk population was stained with antibodies to P-S6 S235/236, P-S6 S240/244, P-44/42 MAPK (Erk1/2), and P-Akt S473 (Cell Signaling), and where applicable stained with donkey anti-rabbit APC (Jackson Immunoresearch) secondary prior to flow cytometry.

Transcription factor staining

In cellular barcoding and Gata3 time course experiments, cells were harvested at indicated time points, washed once, and fixed in FoxP3 Fixation buffer (eBiosciences). Cells were permeabilized with FoxP3 permeabilization buffer (eBiosciences). Where applicable cells were barcoded by staining with Pacific Blue succinimidyl ester (Thermo Fisher / Molecular Probes), and washed. Cells were stained with antibodies to Gata3, Foxp3, and Bcl6 and analyzed by flow cytometry.

DATA ANALYSIS

All flow cytometry data was acquired on a BD LSRII or Fortessa and analyzed using FlowJo (Treestar).

DT40 Transfections

20 million cells were resuspended in a 0.4 cm cuvette (Invitrogen) info transfection media (DT40 culture media excluding pen-strep). 67ug/ml of plasmid (pEGFP-N1-Rasgrp1-EGFP, with either WT Rasgrp1 or the point mutations for R271E or R519G) was added to the cuvette and cells were electroporated using a Biorad Gene Pulser XCell. Plasmids were originally described in Iwig et al. (2013). After a 6 hour recovery, cells were treated with vehicle or the indicated inhibitor for 30 minutes, fixed with 2% paraformaldehyde, washed, and permeabilized overnight at −20°C in 90% methanol. The following day cells were prepared for flow cytometry as described above.

Inhibitors

Rapamycin was purchased from EMD Millipore. For *in vivo* experiments was diluted in DMSO (15.4%), Cremophor (15.4%) and water (69.2%); mice were injected intraperitoneally with 0.4mg/kg rapamycin on days 0, 1, 2, 3, 5, and 7, and cells were harvested on day 8. For *in vitro* experiments, rapamycin (EMD Millipore) was diluted in DMSO and used at 20 nM. BI-D1870 was purchased from Enzo Life Sciences (BML-EI407-0001) and used at 2uM.

Immunoblotting

Relevant murine primary cell populations were isolated by MACS purification (Miltenyi Biotec) or sorting (BD FACS Aria) as indicated. Cells were kept ice-cold throughout the entire procedure. Following purification of the cell population of interest, cells were washed and cell suspensions in PBS were directly lysed in 4X Laemmli buffer. Lysates were clarified by ultracentrifugation (30 minutes at 100,000rpm). Lysates were run 4%–12% gradient Bis-Tris gels (Thermo Fisher), transferred to PVDF membranes, blocked in 3% BSA, and probed for indicated proteins with primary antibodies. Primary antibodies were purchased from Cell Signaling (TBP) and Santa Cruz Biotechnologies (Gata3). Signal was detected using HRP-conjugated secondary antibodies and blots were developed using Supersignal West Pico Chemiluminescent Substrate (Pierce). Images were recorded using a chemiluminescent imager (Fuji LAS-4000).

qPCR

Lymph nodes from 3 mice per genotype were extracted and pooled. Naive CD4^{+} T cells were sorted as described to > 95% purity by CD5 protein level, 30% CD5^{low} and 30% CD5^{high}. Total RNA was extracted from sorted cells using Trizol, the PicoPure® RNA Isolation Kit (ThermoFisher Scientific, KIT0214), and treated with DNase I (ThermoFisher Scientific,12185010). cDNA was generated by reverse transcriptase using the Super Script IV first-strand synthesis kit (ThermoFisher Scientific,18091050). For mRNA gene expression assays, TaqMan primers/probes were purchased from Life Technologies (*CD44* (Mm01277161_m1), and *Gata3* (Mm00484683_m1)), and were normalized to an endogenous control (primer/probe for Ppia (Mm02342430_g1). TaqMan real-Time PCR was performed using TaqMan Fast Advanced Master Mix (Applied Biosciences, 4444963). Multiplex Taqman reactions were run on a QuantStudio 12K Flex Real-Time PCR System (ThermoFisher) in triplicate. The level of transcript expression is presented as a comparison of between CD5^{low} and CD5^{high} populations, of the same sort, calculated as $2^{-\Delta CT}$, where ΔCT is equal to the difference of the proband cycle threshold (CT) between CD5^{high} - CD5^{low}, after being normalized to *Ppia* levels respective to each sample.

Total RNA Sequencing and Ribosome Profiling

Cell Isolation

CD4^{+} CD25^{-} T cells from pooled from LN of multiple WT and Anaef mice were isolated to high purity (> 97%) with the MACS mouse naive CD4+ T cell isolation kit (Miltenyi Biotec).

Total mRNA Sequencing

Total RNA was isolated from 20,000 cells per sample using the Dynabeads mRNA DIRECT Purification Kit (Thermo Fishcer Scientific) following manufactors protocol. Libraries were prepared using the Nugen/Nextera XT kit (Illumina) and single-end 50pb RNA sequencing was performed using a HiSeq 4000 (Illumina).

Ribosome Profiling

The bulk pool of purified $CD4^+$ T cells (60-100 million cells) were washed in RNase-free PBS, treated with 100ug/ml cycloheximide (CHX) for 1 minute, and then lysed in polysome lysis buffer (20mM Tris 7.5, 250mM NaCl, 15mM MgCl2, 1mM dithiothreitol, 8% glycerol, supplemented with 0.5% triton, 30 U/ml Turbo DNase (Ambion) and 100μg/ml cycloheximide), as described in Stern-Ginossar et al. (2012). Lysate was clarified by centrifugation (10 minutes, 20000 g, 4°C), snap-frozen, and RNA content was measured using the Qubit RNA HS Assay Kit (Thermo Fisher Scientific). Ribosome protected fragments (RPFs) were prepared by digesting samples for 1 hour at room temperature with 8ug micrococcal nuclease (MNase) per ug of RNA, 5mM CaCl2, 1:10 SuperAseIn (Invitrogen), and reactions were stopped with 6.25mM EGTA. RPFs were purified by sucrose cushion by overlaying MNase-digested lysate onto sucrose solution (34% sucrose, 5X polysome buffer, 50mg/ml CHX, 1M DTT) and ultracentrifugation was performed in a TLA-100.3 rotor (Beckman-Coulter) for 1 hour at 100,000rpm, 4°C. Subsequent sample clean up and library preparation was performed using the TruSeq Ribo Profile (Mammalian) kit (Illumina) and libraries were sequenced on a HiSeq 4000 (Illumina) in the UCSF Center for Advanced Technology Core.

Data Analysis

Total RNA was aligned to the mouse genome (NCBI build 38, GRCm38) using TopHat v1.4.1 (Trapnell et al., 2009). Ribosome Protected Fragment sequences were aligned to the mouse genome (NCBI build 38, GRCm38) using TopHat v1.4.1 (Trapnell et al., 2009) following rRNA contaminant removal using Bowtie v0.12.7 (Langmead et al., 2009). Length distribution was determined using Samtools v0.1.18 (Li et al., 2009); metagene analysis, masking of first and last 5 codons, and RPKMs (reads per kilobase million) were calculated using Plastid (Dunn and Weissman, 2016). Differential expression was performed using DESeq2 (Love et al., 2014). Functional annotation clustering was performed using DAVID v6.8 (Huang et al., 2009). The 3000 genes highest and lowest log2FC in a given list were input and compared to background, which was set as all the genes in that given list. Pathways shown had an enrichment score of 2 or greater.

QUANTIFICATION AND STATISTICAL ANALYSIS

Information on statistical tests, the value of "n," what "n" consists of, and the precision measures for each experiment can be found in the corresponding figure legends for each experiment. Statistical tests were carried out in Prism, with ns defined as $p > 0.05$; * as $p \leq 0.05$, ** as $p \leq 0.01$, *** as $p \leq 0.001$, and **** as $p \leq 0.0001$.

For mouse studies, within an experiment animals of the same age were used unless otherwise indicated in the figure legend, and both male and female animals were used. For *in vivo* experiments, littermate controls of both genders were randomized into vehicle and rapamycin treatment groups such that equivalent numbers of mice of each gender received each type of dosing.

DATA AND SOFTWARE AVAILABILITY

The accession number for the ribosome profiling and RNA Sequencing data reported in this paper is GEO: GSE114741.